Research Square

Preprints are preliminary reports that have not undergone peer review.
They should not be considered conclusive, used to inform clinical practice,
or referenced by the media as validated information.

Amniote traits and terrestriality in an early amphibian

Michael Coates

mcoates@uchicago.edu

University of Chicago https://orcid.org/0000-0003-2843-1075

Benjamin Otoo

Earth Sciences Department, Carleton University

Abigail Caron

University of Chicago https://orcid.org/0000-0002-0906-8218

Kristen Tietjen

University of Chicago

Marcello Ruta

University of Lincoln https://orcid.org/0000-0002-6151-0704

Biological Sciences - Article

Keywords:

Posted Date: March 6th, 2026

DOI: https://doi.org/10.21203/rs.3.rs-9013156/v1

License: This work is licensed under a Creative Commons Attribution 4.0 International License.
Read Full License

Additional Declarations: There is **NO** Competing Interest.

Amniote traits and terrestriality in an early amphibian

Michael I. Coates[1], Benjamin K. A. Otoo[2], Abigail Caron[1,3], Kristen Tietjen[4], Marcello Ruta[5]

[1] Department of Organismal Biology and Anatomy, University of Chicago, Chicago, IL, USA.

[2] Department of Earth Sciences, University of Carleton, Ottawa, Ontario, Canada.

[3] Committee on Evolutionary Biology, University of Chicago, Chicago, IL, USA.

[4] Biodiversity Institute & Natural History Museum, University of Kansas, Lawrence, KS, USA.

[5] Department of Life Sciences, University of Lincoln, Lincoln, UK.

Correspondence to: Michael I. Coates, mcoates@uchicago.edu

Abstract

The origin of terrestrial tetrapods is linked to the evolutionary split between amniotes, which occupied dryer upland environments, and stem tetrapods and lissamphibians which diversified into wetlands[1-3]. Skeletal evidence of early lissamphibian habits includes broad-based skulls with sensory lateral lines, gill bars, pharyngeal teeth, and weakly ossified vertebrae[4-6]. In contrast, early amniotes generally exhibit narrow-based skulls, well ossified postcrania, and limbs with evidence of claws[7,8] implying presence of keratinized, resilient, watertight skin[9,10]. However, histological and molecular genetic analyses of extant tetrapods find keratinization-linked processes shared throughout the crown clade, suggesting their presence in the stem-group as well[11-13]. But fossils have thus far provided no direct support for this possibility. Here, we report unusually complete remains of the stem-lissamphibian *Eugyrinus wildi* from the Upper Carboniferous (~319 million years ago) of Lancashire UK. The specimen displays clawed limbs, regionalized scaly skin, eyes adapted for subaerial vision, and gut contents including terrestrial prey. In addition to supporting the stem-tetrapod keratinization hypothesis[11-13], these new data imply that adults of the last common ancestors of living tetrapods were terrestrially adapted even though early life history stages remained tied to aquatic conditions[4,6,14]. Further, these findings emphasize the derived condition of modern Lissamphibia, suggest emergent behaviours of early temnospondyls in coal swamp habitats, and question the value of early claw-marked fossil trackways as definitive evidence of crown group amniotes and, therefore, as calibrations in tetrapod phylogeny[15].

Main text

The tetrapod colonisation of diverse terrestrial environments is primarily associated with early members of the amniote lineage[16]. Key innovations linked with this shift include the evolution of a cleidoic egg[17] and the emergence of cornified (keratinized) skin[12]. Both provide barriers against dehydration, contribute

to thermoregulation, and protect against mechanical damage, allowing survival in drier environments relative to the wetland and aquatic habitats of their lissamphibian and stem-tetrapod relatives[18]. However, eggs and integument rarely fossilize. No direct evidence of a Palaeozoic cleidoic egg has yet been found, and the earliest shell fragments are mid-Mesozoic[19]. Nevertheless, fossilized amniote skin is now known from the early Permian[10] and records of amniote limbs with claws track keratinized outgrowths back to at least the late Carboniferous[7,20] and perhaps earlier[15,21-24], consistent with arguments supporting the significance of claws in the initial phases of terrestrialisation[11]. But cornified skin appendages are not unique to amniotes. Lissamphibian adult skin includes a keratin monolayer occasionally ornamented with horns and 'denticles'[25,26], and certain frogs and salamanders bear claws[11,25-27]. Even though these claws are histologically distinct[27], there is mounting evidence that amniotes and lissamphibians share an ancestral keratinizing process. This process is hypothesized to have originated in stem tetrapods via a shared genetic program evolved to resist and regulate the epidermal response to biomechanical stress and damage, particularly to the plantar surfaces of feet and toe tips[11-13].

Thus far, material from the growing fossil record of non-amniote early tetrapods has neither supported nor refuted these arguments. The diagnostic traits attributed to early amniotes have remained largely unchallenged. Here we present new evidence and perspectives on these questions revealed by microcomputed tomography (µCT) of the long-known type and only specimen of the Pennsylvanian (Bashkirian; ~ 319 Myr) tetrapod *Eugyrinus wildi* (MANCH:W.1222: Fig. 1)[28-32] from the Soapstone Bed of the Burnley coalfield at Carry Heys coal pit, Trawden, northwest England[33]. The specimen occurs in a nodule, split into part, counterpart, and cranium (Extended Data Fig. 1a,b). Total length, from snout to end of incomplete tail, is 80mm. Morphological data were obtained from µCT scans and nodule surfaces dusted with ammonium chloride, the latter highlighting complete scale cover and gut contents (Figs 1a and 2c). The forelimbs and hindlimb (Figs 1 and 2a,b and Extended Data Fig. 2)

reveal evidence of claws in one of the earliest members of the Temnospondyli[4-6,32], a group widely associated with the lissamphibian stem[1,31,34,35] although alternative hypotheses place them on the tetrapod stem[36]. Under both interpretations, *Eugyrinus* supports arguments for an ancestral keratinizing process common to all extant tetrapods, with functional implications for scenarios of tetrapod terrestrialisation in general and for *Eugyrinus* in particular. Additionally, consistent with other fossil vertebrates from the same locality[37-40], *Eugyrinus* preserves soft tissues including neural material of the eyes, nose, and spinal cord (Fig. 2d–f and Extended Data Fig. 3). Combined, these data provide unprecedented insights into the palaeobiology of this diminutive amphibian.

Description

Skeletal anatomy

The most recent description of the skull[31] is largely confirmed, including jugal-lacrimal contact (Extended Data Fig. 4a,b), broad interpterygoid vacuities (Extended Data Fig. 5) and presence of sulci for cranial lateral lines (although the supratemporal-postorbital line was not found) (Extended Data Fig. 4c,d). Some indication of the occiput is preserved as a natural mould (Extended Data Fig. 4d). The dermal ornament is mostly finely pitted suggesting that the specimen is subadult[6] consistent with previous interpretations[31,32]. New data from µCT scans concern the anterior the palate and scleral ossicles (Fig. 2e and Extended Data Figs 3b,d and 5).

The parasphenoid cultriform process is broad (width to length ratio ~1:7), toothless, and, from the extent of the deeply recessed midline suture between the vomers, appears to reach almost as far as the rear of the missing premaxillae (Extended Data Fig. 5b). The vomer forms the anterior rim of each palatal vacuity. Denticles are mostly confined to the outer margins, arranged in rows that flank the choana (Extended Data Fig. 5c) and extend around the base of two vomerine fangs. The Y-shaped palatine (Extended Data Fig. 5c,d) encloses the rear of the choana and bears a further, larger, fang pair. In

dorsal view, the vomer, anterior to the choana, supports a hemi-conical septomaxilla flaring towards the external nares[41,42] (Extended Data Fig. 5d). The rear of the choana is bordered by a broad, anteriorly concave, palatine ridge. Scleral ossicles have sunk deep within each orbit (Figs 1a,c and 2d,e and Extended Data Figs 3e-h and 5b). The complete ring includes around thirty plates, matching an estimated general condition for temnospondyls[45]. Ossicle size varies such that the upper circumferential half is composed of ten large and the lower of twenty much smaller plates. Consistent with previous descriptions[30,31] the lower jaw (Extended Data Figs 4b, 5a, and 6a) bears a coronoid process with a surangular component, and retroarticular process posterior to the glenoid. Sulci bordering the rear of the surangular and angular signal presence of a mandibular lateral line. The adductor fossa extends for around 30% of jaw length, compared with ~25% in *Trimerorachis*[43] and *Dendrerpeton*[44]. The proximal portion of the right stapes shows a stapedial foramen, part of a stapedial groove, and the slender base of shaft bearing the edge of a muscle scar (Fig. 2d and Extended Data Fig. 6b). The shape matches that of *Balanerpeton*[14] and *Dendrerpeton*[46]. In life the shaft likely connected with a small tympanum and served to conduct airborne sound. Unlike many other temnospondyls[4,5,47], the pharyngeal region shows no branchial arches or pharyngeal teeth.

The axial skeleton of 28 presacral vertebrae is incompletely ossified: neural arch halves and spines are separate and centra are absent (Fig. 1; Extended Data Fig. 1c). Neural spines are subrectangular; zygapophyses and parapophyses are incompletely developed. A single sacral vertebra precedes the 12 caudal vertebrae of the incomplete tail. Left- and right-side rib series are mostly intact. Vertebra 3 bears the anteriormost rib, the following 5 pairs are stout and expanded proximally and distally; rib heads are broad but not obviously bicipital. Maximum rib length occurs around vertebrae 7 and 8; the sacral rib is short but well ossified and dorsoventrally deep (Fig. 1). Caudal ribs lack any sign of distal expansion.

The pectoral girdle includes ossified cleithra, clavicles, an interclavicle, and scapulocoracoids (Extended Data Fig. 6c). The ossified portion of each scapulocoracoid shows a large supraglenoid foramen; coracoid and articular portions are unknown. Dorsally, the slender cleithrum bears a flag-like anterior lamina like that of *Dendrerpeton*[48]. The pelvic girdle lacks an ossified pubis and the ilium and ischium are separately ossified (Extended Data Fig. 6d). The iliac blade is simple, with a near-straight anterior margin. The smooth medial face of the ilium shows no ridge marking the sacral articulation. The ischial plate is small, subtriangular, and fans out from an ossified dorsal margin.

The limbs are well preserved. CT scans reveal both forelimbs and the left hindlimb as barely disturbed from in-life articulated condition (Figs 1 and 2a,b; Extended Data Fig. 1c). Each forelimb includes humerus, radius, ulna, and digits, but no ossified wrist (Figs 1 and 2a and Extended Data Figs 2a-d). Proximal and distal heads of long bones are absent. The ossified portion of the humerus corresponds to the length of around four trunk vertebrae, with around ninety degrees of torsion between long axes of the expanded heads. A large entepicondylar foramen lies distal to the waist of the humeral shaft (Extended Data Fig. 2c). The radius and ulna are about two thirds humeral length. The ulna is slightly longer than the radius. The radius is more substantial than the ulna, and broader distally. The four-digit manus has a phalangeal formula of 2.2.3.3 (Fig. 2a and Extended Data Fig. 2d). The digits are long: digit three exceeds humerus length, and the terminal phalanges resemble those of the eureptile *Anthracodromeus*[7]. Each terminal phalanx is elongate, slender, laterally flattened, and gently curved but with the curvature radius reduced sharply towards the tip. Unlike the ‘very abbreviated elements’ of *Balanerpeton*[14], the close resemblance of the terminal phalanges to the unguals of *Anthracodromeus* leads us to interpret these digits as claw bearing.

The hindlimb includes femur, tibia, fibula, and a five-digit pes; the ankle is unossified (Fig. 2b and Extended Data Figs 2e–i). The ossified portion of the femur is between five and six mid-trunk vertebrae in length. Tibia and fibula are little more than half femoral length. The tibia, slightly longer and stouter

than the fibula, has a broad proximal head. The phalangeal formula of the pes is 2.2.3.4.3 (Extended Data Fig. 2h). The toes are long: digits III and IV exceed femoral length. The linear dimensions suggest a footprint of about double the area of the manus. The pes closely resembles that of the eureptile *Anthracodromeus*[7]. It shares the phalangeal formula, and digit V is directed laterally away from digits I-IV as in many amniote hindlimbs. Each terminal phalanx is slender, laterally flattened, increasingly curved towards the distal tip (Extended Data Fig. 2i), and approaching the length of the penultimate phalanx (Extended Data Table 1). These near-hooked terminal phalanges resemble unguals and, again, signal the presence of claws.

Dermal scale coverage is complete, regionalised, and preserves three-dimensional relief. The small dorsal scales (Fig. 2e) are aligned in dorsoventrally directed rows – at least four per axial segment. Anterior trunk scales are smaller than those of the caudal region (around 60% of linear dimensions); each is thinly ossified but has a distinct central boss. Scales are almost rhombic with a slightly convex posterior margin, unlike the 'round-oval' scales characteristic of other temnospondyls[47,49,50]. Trunk scales show no trace of a posterior lateral line canal or groove (persistence of free neuromasts in the overlying skin is possible, cf. the caecilian *Ichthyophis*[51]). Hindlimb dorsal scales are varied in shape, with broad scales overlying the knee joint (Fig. 1a). Gastral scales[49] are large, ovoid, and convex with circumferential growth lines.

Soft tissues

Tomograms of *Eugyrinus*, like those of *Coccocephalus*[37] and *Trawdenia*[40] from the same locality, show soft tissues preserved as radiodense material relative to surrounding matrix (Extended Data Fig. 3a,c). Cranial material of the central nervous system extends anterolaterally from the forebrain, whereas postcranial material occupies the neural arches in sections of the axial skeleton. The cranial material preserves an olfactory tract reaching the right nares and choana (Fig. 2e and Extended Data Fig. 3a,b,d),

forming a dorsolaterally directed hemispherical cup at the narial opening. Its short neck, interpreted as the tubular vestibulum, is held by the septomaxilla. Proximally, this neck expands laterally into an incomplete ventrally open nasal sac that fills the shallow bowl surrounding the dorsal margin of the choana, formed partly by the palatine-vomer ridge[42]. The postcranial neural material occupies the neural canal as solid infill, exposing smooth surfaces between neural arches (Fig. 2f).

Three-dimensional traces of the eye are preserved in the right orbit (Fig. 2c and Extended Data Fig. 3e–h). Again, similar preservation is evident in other Carry Heys material[38,40]. The eyeball forms a dome with an apical pit (Extended Data Fig. 4a), CT slices of which are extremely radiodense (Extended Data Fig. 3c). Within the dome, a less radiodense toroidal zone is seated above the collapsed ring of scleral ossicles. Proximal to these, a membrane with central dimple encloses the mesial boundary of the eyeball. This resembles a retinal pigment epithelium (RPE)[52], including an incomplete area which likely marks the optic nerve entrance. The daisy-petal arrangement of scleral ossicles around the RPE (Fig. 2d and Extended Data Fig. 3e–h) is deceptive: the ossicles have rotated inwards so that the inner circumference is now proximal to the outer perimeter. Inner (toroidal) and outer (apical) clouds of radiodense material appear to be pyritic infill of the vitreous and aqueous humours. This suite of materials preserves the convex external profile of the original eyeball.

Phylogenetic relationships

We added *Eugyrinus* to Gee's[53] (see also Gee & Sidor[54]) amended version of Schoch's[55] data matrix to investigate its phylogenetic position within temnospondyls. The embolomere *Proterogyrinus scheelei*[56] and the colosteid *Greererpeton burkemorani*[57,58] were included as outgroups. The matrix was subjected to non-calibrated Bayesian analysis and a suite of six parsimony analyses using different combinations of character ordering and weighting (Methods). In agreement with recent studies[35,44,53], all analyses retrieve Dvinosauria as the sister clade to other temnospondyls and, also

consistent with prior hypotheses[5,31,32,44,59], *Eugyrinus* is placed as the sister taxon to other dvinosaurs (Fig. 3 and Extended Data Fig. 7 and Supplementary Information). In the single shortest tree yielded by four out of the six parsimony analyses, the dvinosaurs, including *Eugyrinus*, are supported by at least 11 character-state changes. Of these, the following synapomorphies are evident in *Eugyrinus*: laterally placed orbits framed by slender jugals; orbit margins lying flush with the skull roof; interclavicle substantially longer than posterior division of skull; unossified humeral heads; unossified carpals; unossified pubis; unossified tarsals. Although unossified conditions are of uncertain systematic value in a subadult individual, the phylogenetic placement is uncontroversial. In the same analyses, character-states uniting remaining temnospondyls (Dendrerpetidae and higher taxa) include the following: posterior extent of the lacrimal restricted to the antorbital region; absence of lateral line sulci in adult crania; transversely elongate basipterygoid process frames posteriorly wide interpterygoid vacuity; 23-28 presacral vertebrae. All listed shared character-states are homoplastic but consistently suggest exclusion of *Eugyrinus* from a more nested location within the Temnospondyli.

Temnospondyl genera approximately contemporaneous with *Eugyrinus* include the *Dendrerpeton*/*Dendrysekos* complex[44,48,60] and *Procochleosaurus*[61], while earlier records are limited to *Balanerpeton* plus fragments of uncertain affinity from the mid Viséan[14,62]. Our results imply that all major temnospondyl lineages originated within the Mississippian (Fig. 3)[63] but raises the question of why the earliest record of the group remains scanty.

Discussion and conclusions

This new picture of *Eugyrinus* anatomy clarifies conditions in the earliest stem lissamphibians and other early tetrapods close to the crown-clade root. Large, clawed feet are not usually associated with temnospondyls, although claw-like terminal phalanges have been recognized in the amphibamid *Doleserpeton*[34] and depicted in the putative dvinosaurian *Bermanerpeton*[47](see Supplementary

Information for remarks on *Bermanerpeton* affinities). Moreover, the hindlimbs of these temnospondyls share similar construction – an elongate femur, short tibia and fibula, and a large pes, though comparisons show *Eugyrinus* to have the proportionaly largest pes. To test for phylogenetic signal among these seemingly distinctive hindlimb proportions we assembled a data set from 67 taxa, drawn mostly from Palaeozoic material and subjected the tripartite divisions (stylopod, zeugopod, and autopod) to a principal components analysis (Fig. 4a and Supplementary Information). But our results show broad overlap between all major tetrapod groups; 'microsaurs'/lepospondyls alone appear restricted to an area defined by a lengthy femur and pes. Against this background, *Eugyrinus*, *Doleserpeton*, and *Bermanerpeton* occupy a modest extremity of temnospondyl limb disparity within what might be described as 'microsaur' territory.

Functionally, it has been argued that early tetrapod toes lengthened in response to the complex demands of terradynamics[64,65]. To further explore the significance of *Eugyrinus* limb data we used methods employed to infer function in the similarly built hindlimbs of the eureptile *Anthracodromeus*[7]. *Eugyrinus* and *Anthracodromeus* share phalangeal formulae, digit proportions, and, based on terminal phalanx shape, similar claws. However, *Anthracodromeus* is interpreted as scansorial[7], a locomotor strategy unconsidered thus far for temnospondyls, although documented in extant amphibians[66,67]. This limb function was estimated from two sets of claw curvature data collected from extant amniotes[68,69] and supplemented with material from late Palaeozoic taxa[7]. Claws (the keratin sheaths) rarely fossilize, but measurements of ungual morphologies in living taxa have been shown to provide conservative signals of claw shape[69,70].

Eugyrinus µCT scans allowed collection of curvature measurements from all five terminal phalanges of the hindlimb (Extended Data Fig. 8 and Methods). Results delivered varied measures of claw curvatures and angles of attack, but digits II-V clustered together well within the territory demarcated by extant and extinct amniotes[7,68,69] (Fig. 4b,c). Digit I is an outlier to digits II-V, as might be

expected from visual inspection (Fig. 4b and Extended Data Fig. 8a). Intriguingly, this is consistent with transcriptomic analyses of amniote digit differentiation showing that the anterior-most digit has a unique, conserved, expression profile[71]. Returning to functional inference, the scatter plot of inner against outer curvatures (Fig. 4b) placed *Eugyrinus* near *Anthracodromeus*, close to many of the fossil amniotes but without a clear functional signature. In contrast, the plot of inner curvature against angle of attack (Fig. 4c) locates *Eugyrinus* data within a region of overlap among scansorial (climbing), gryporial (grasping) and cursorial taxa, again close to *Anthracodromeus*. This result shows that these terminal phalanx shapes at least approximate claws adapted for terrestrial use. For these reasons, we suggest that *Eugyrinus* claws might have been employed for gaining a purchase on irregular surfaces and clambering through structurally complex marginal habitats.

As for the inferred presence of claws, this implies integument keratinization – an adaptation long associated with enhanced resistance to dehydration and the amniote colonisation of dry land[11]. Further to this, claws have been considered unique to crown-group amniotes[15], although claw-bearing stem-group amniotes might include *Limnoscelis*[22], *Orobates*[72], *Bromerpeton*[24], and *Termonerpeton*[23]. Against this background, *Casineria*[21] deserves particular attention: described as having “unguals which are curved ventrally into claws”, its terminal phalanges match those of *Eugyrinus* (Extended Data Fig. 8e,f). Functionally, claws supply not only traction, but also protection from wear and tear. The water-to-land transition exposed integument to new biomechanical stresses, especially the weight-bearing plantar surfaces. Such stresses undoubtedly resulted in epidermal changes: repair and regionally enhanced regeneration leading to a thicker stratum corneum. An increasing range of data on the generative and regulatory mechanisms underlying these features[11-13,73] place the origin of these systems (leading to limbs with claws or keratinized digit tips) on the tetrapod stem. Predictably, the fossil record of such integumentary structures lags behind wide-ranging phylogenetic inferences drawn from neontological data alone, despite exceptional discoveries[10,74]. Here, *Eugyrinus* delivers morphological corroboration of

this phylogenetically deeper origin, irrespective of whether temnospondyls are considered stem-group lissamphibians or stem-group tetrapods[1,34-36].

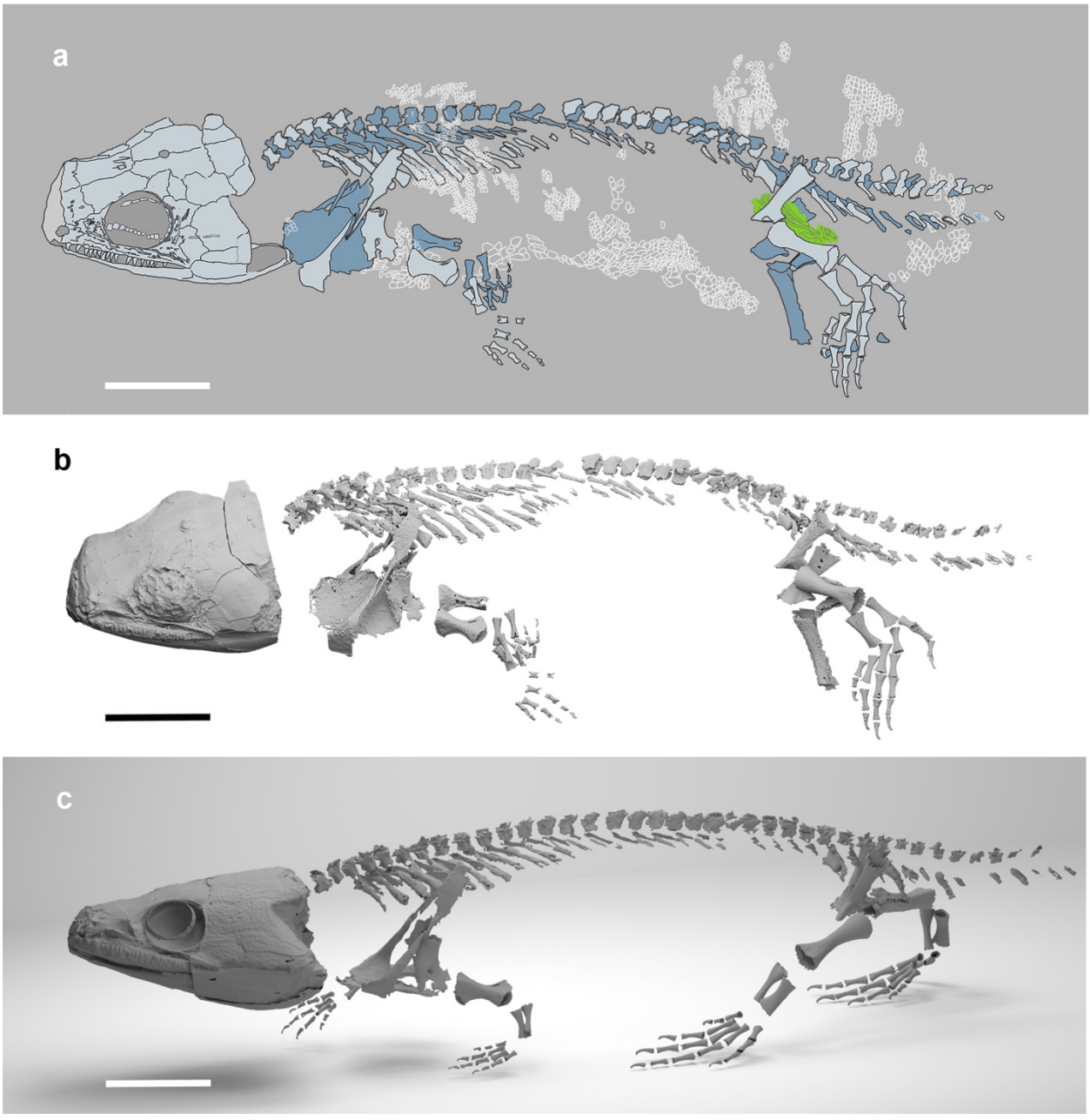
The extent of skin keratinization in *Eugyrinus* is unknown in comparison with modern amphibians[25,26]. Nevertheless, we consider it significant that its dorsal scales (mineralised dermal scales rather than cornified epidermal scales) differ strongly from those of other temnospondyls (thin, ovoid, and with considerable overlap[14,47,49,75]) and stem tetrapods (large and similarly proportioned to gastral scales[50]). Rather, the small size (both absolute and relative to gastral scales) and 'cobbled' texture converge on that of the squamation of modern lizards where roughness provides camouflage via diffusion of reflected light as well as assisting friction-assisted locomotion[76] (Fig. 2e).

Three further pieces of evidence support our inference that *Eugyrinus* engaged in substantial terrestrial activity: the stapes, eyes, and the gut contents (supplementing the already noted absence of evidence for a gill skeleton). The stapes conforms to the rod-like form associated with perception of airborne sound[14]. The three-dimensionally preserved eye with convex external profile (Fig. 2c and Extended Data Fig 3b,d–g) provides some indication of an air-cornea interface with the refractive properties required for subaerial vision[77]. A cornea serves as both protective layer and lens, focusing light on the retina[78]. The 'buena vista' hypothesis[79] used orbit size as a proxy for eye size and improved visual performance just preceding the tetrapod water-to-land transition. The consequent vast increase in sensory input, especially distance vision, was linked to the emergence of more elaborate action sequences and corresponding evolution of the nervous system. But here we show evidence for an eye with improved acuity for seeing through air as well as a likely focus of such visual attention: fragments of a palaeodictyopteran nymph. Located within the rear of the abdominal cavity[80] (Fig. 1a), these remains have already been characterised as the 'exceedingly satisfactory evidence'[30] that *Eugyrinus* shared the insectivorous habits of many extant amphibians.

In summary, *Eugyrinus* offers a novel perspective on the terrestrially adapted conditions and sensory ecology of a near-adult temnospondyl branching close to the base of the clade. Although retaining aquatic adapted cranial lateral lines and large olfactory apparatus[81], the material supports the hypothesis that the lineage as a whole originated with terrestrial adults[14]. This revised picture further suggests that integument keratinization and claws were variably expressed throughout early tetrapods including stem members; thus not restricted to amniotes. These findings in turn raise questions about the clade assignment of Palaeozoic tetrapod trackways. Tetradactyl manus imprints have long been attributed to temnospondyls and often show blunt, rounded, digit tips, but examples[82,83] also exhibit terminal impressions with scratch marks or digit escape traces (*Batrachichnus*, *Characichnos*, *Hylopus*, *Palaeosauropus*) that might result from limbs like those of *Eugyrinus*. If claws, rudimentary or otherwise, are scattered throughout early tetrapods, then the Tournaisian trackways attributed to crown-group amniotes[15] deserve re-evaluation, and post-Devonian, rather than Eifelian-Frasnian, estimates of crown tetrapod origin[35,84] remain plausible.

The evolutionary impact of integument keratinization was likely widespread across early tetrapods. Although thickened, cornified, scaled skin is a key derived feature of amniotes –conferring resistance to water loss, mechanical stress, injury, and ultraviolet radiation– we propose an earlier role in which the environmental tolerance conferred by keratinization offered a selective advantage among taxa exploring diverse water-to-land transitions, potentially shaping the survivorship of clades navigating the environmental crises surrounding the end-Devonian mass extinction[85].

297 **Figures and Figure Legends**
298



299
300 **Fig. 1 The skeletal anatomy of *Eugyrinus wildi*. a,** The holotype MANCH:W.1222, mapped, combining
301 data from exposed surfaces of cranium, part and counterpart, with µCT data. Colour code: blue with
302 black outline denotes skeleton; pale blue near side, dark blue far side; white outline denotes
303 squamation; green indicates gut contents. **b**, Rendered µCT data showing skeletal morphology and
304 posture as preserved in nodule; postparietal, occipital region of skull, and rear of lower jaw, absent from
305 scans. In both images combined data rotated horizontally to show anterior to left. **c**, Skeletal
306 reconstruction with minimal restoration (skull composite from natural moulds of external and mesial
307 surfaces; hindlimb skeleton mirrored) in lateral view; scales omitted. Scale bars 10 mm.
308

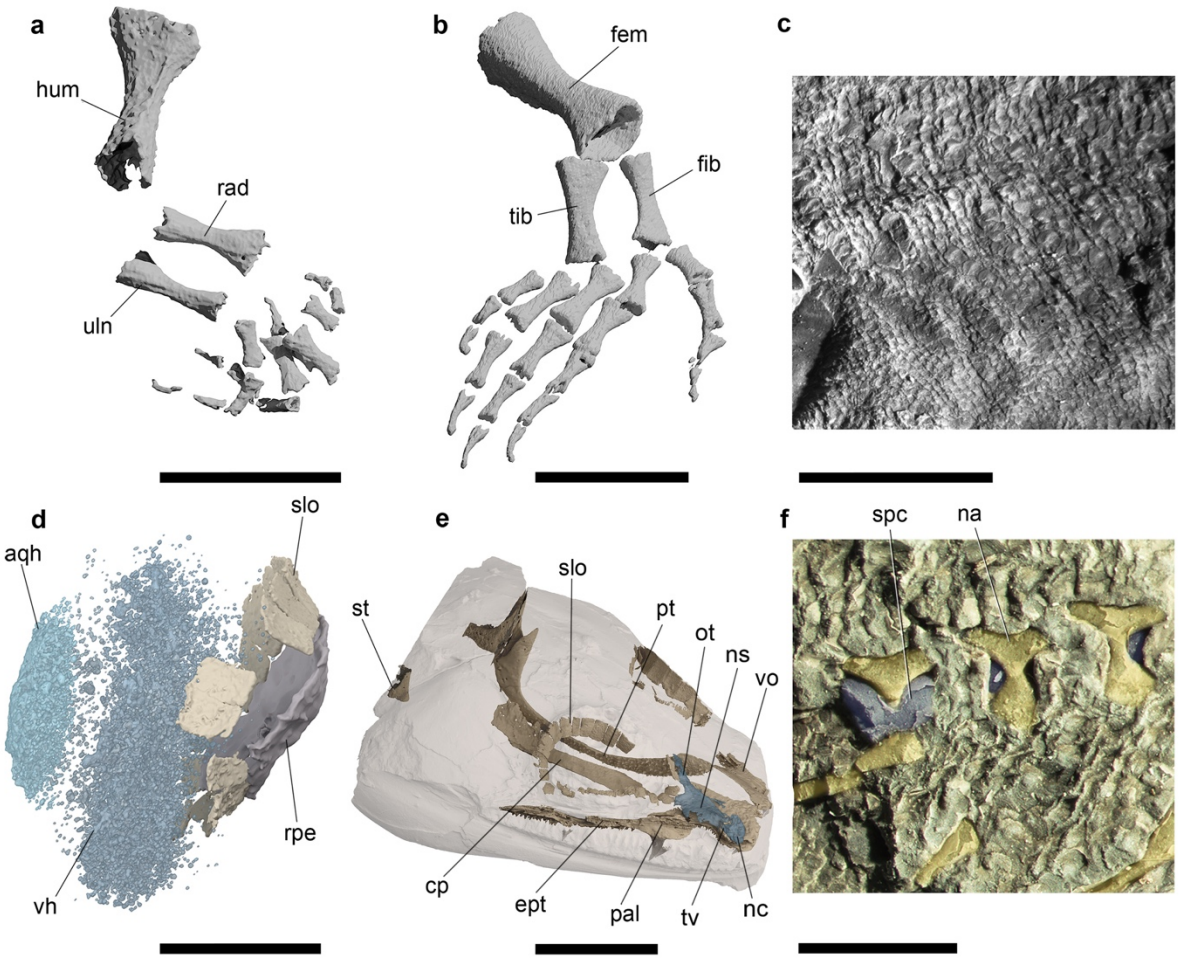


Fig. 2. Morphological details of *Eugyrinus wildi* (MANCH:W.1222). **a**, Left forelimb. **b**, Right hindlimb. **c**, Anterior flank scales. **d**, Right eye, rendered from radiodense material and scleral ossicles in anterior aspect. **e**, Cranium with rendered radiodense material and skeletal detail showing olfactory tract and nasal sac, palate, and scleral ossicles in dorsolateral aspect. **f**, Neural arches (mineralised cores, hence waisted shapes) from the mid trunk enclosing spinal cord. aqh, aqueous humour; cp, cultriform process (parasphenoid); ept, ectopterygoid; fem, femur; fib, fibula; hum, humerus; na, neural arch; nc, nasal capsule; ns, nasal sac; ot, olfactory tract; pal, palatine; pt, pterygoid; rad, radius; rpe, retinal pigment epithelium; sc, spinal cord; slo, scleral ossicles; st, stapes; tib, tibia; tv, tubular vestibulum; uln, ulna; vh, vitreous humour; vo, vomer. Scale bars, 5 mm (**a**,**b**,**d**,**e**) and 2.5 mm (**c**,**f**).

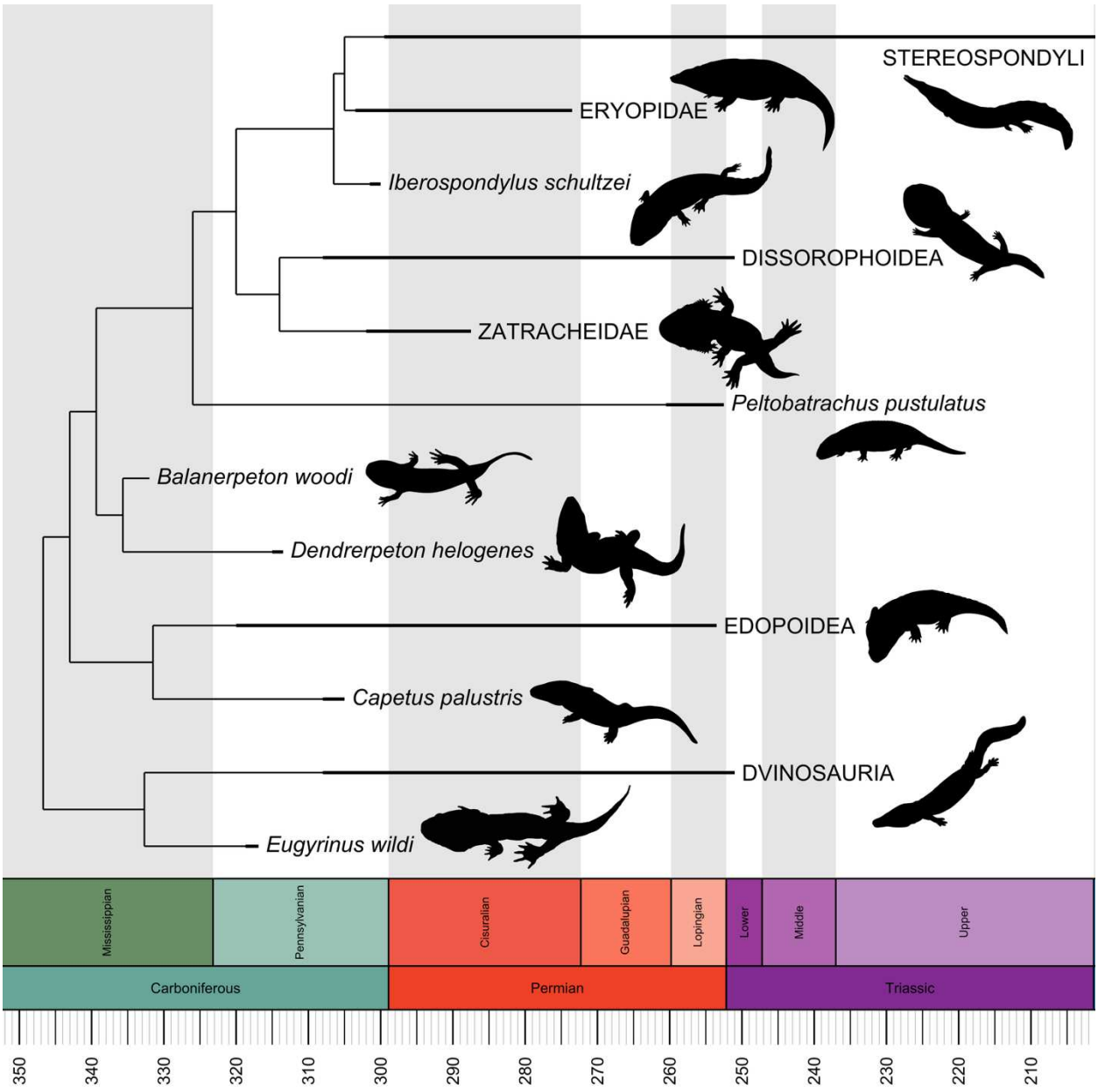


Figure 3. Phylogenetic position of *Eugyrinus wildi*. Time-scaled phylogenetic tree; see Extended Data Fig. 6 for complete results using maximum parsimony and Bayesian analyses, and Supplementary Information for details on phylogenetic analyses. Silhouettes except *Eugyrinus* are adapted from Phylopic under Creative Commons licence CC0 1.0.

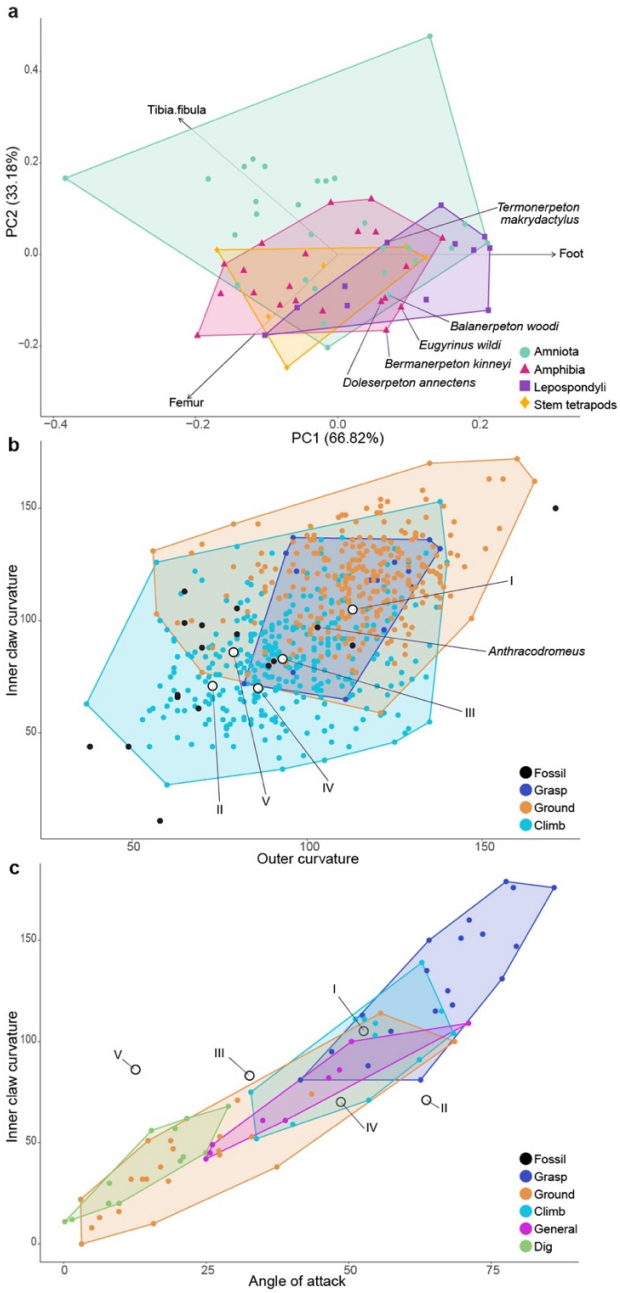
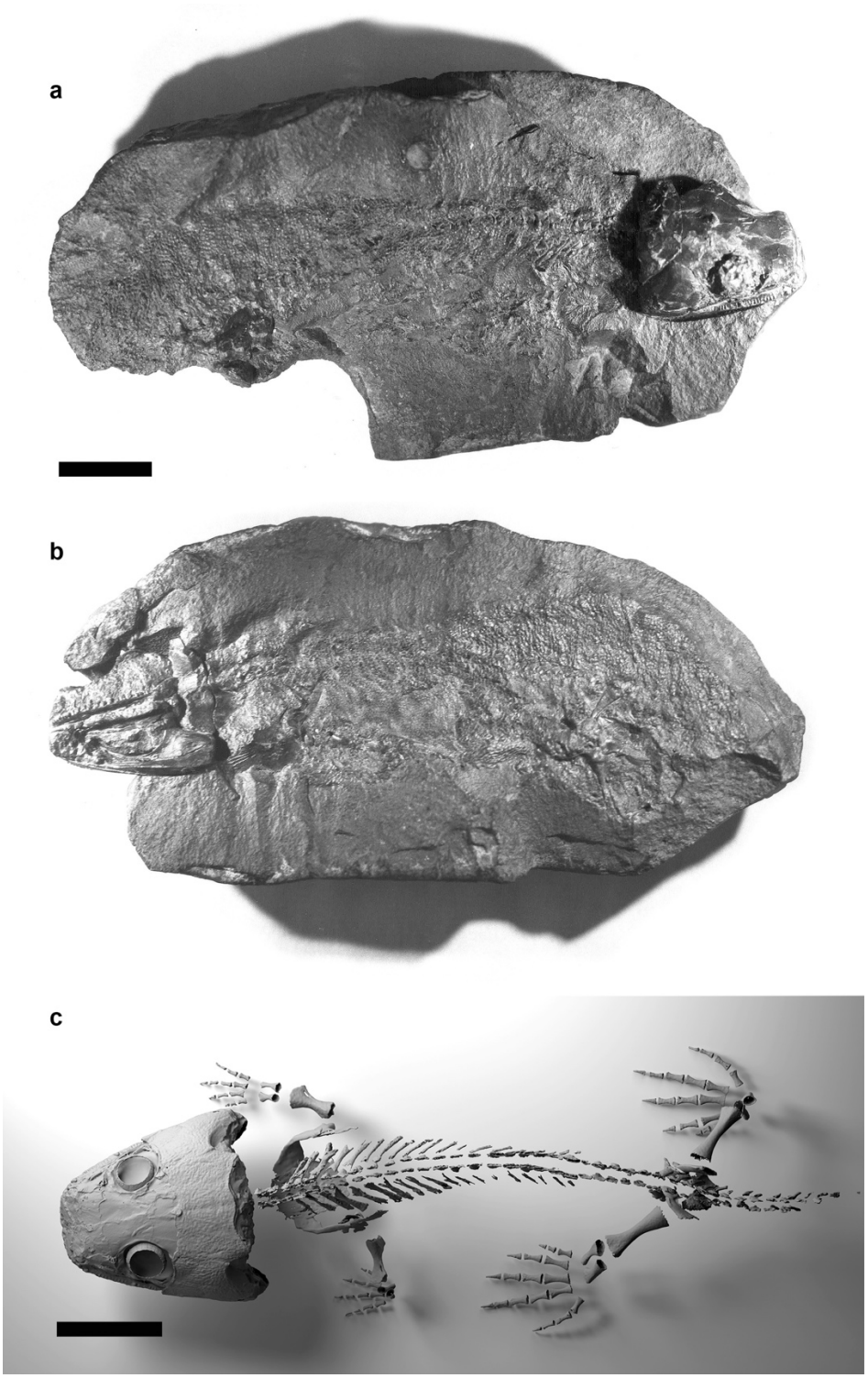
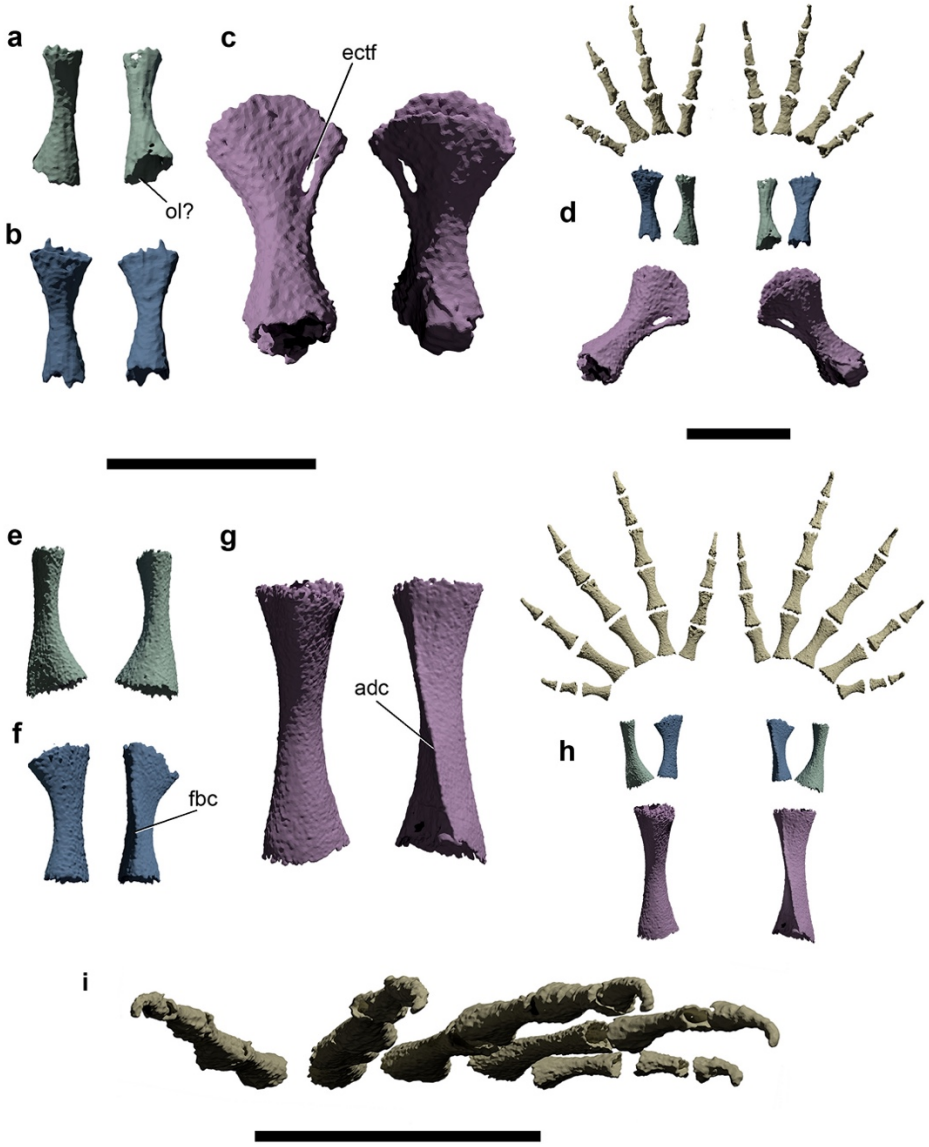


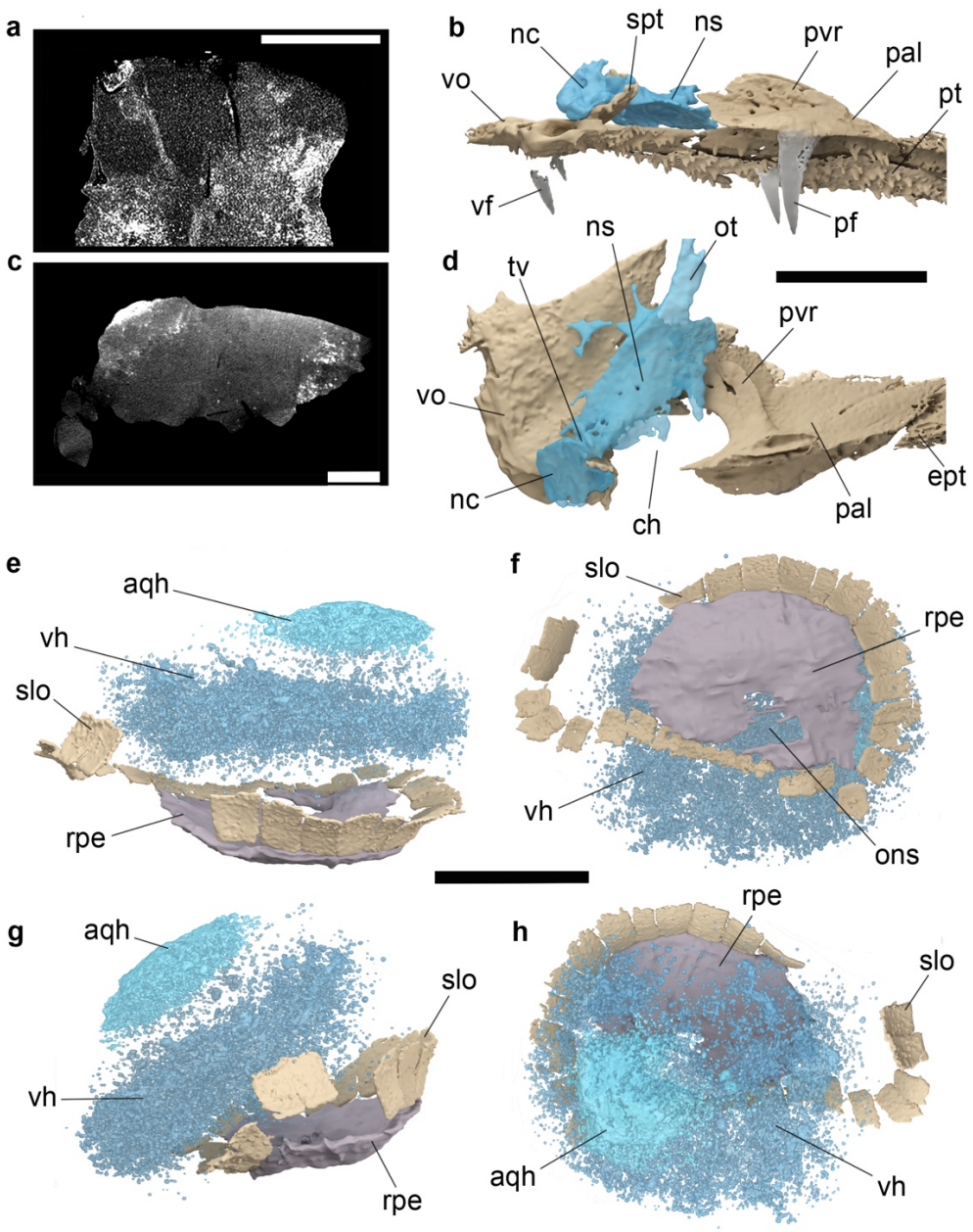
Figure 4. Morphometric analyses of limb proportions and terminal phalanges/claws. a. Morphospace of 67 early tetrapod digit-bearing hindlimb proportions (stylopod, zeugopod, autopod) based on first two principal components (numbered taxa listed in extended data table 1). **b**,**c**, Terminal phalanx and claw morphospace. **b**, Scatter plot of claw inner curvature vs. outer curvature, hulls enclose data linked to extant taxa claw behavioural function from Birn-Jeffery *et al*.[68]; black dots to fossil taxa (digit 3) from Mann *et al*.[7] figure 4C; Roman numeral dots to terminal phalanges of digits I-V in *Eugyrinus*. **c**, Scatter plot of claw and terminal phalanx inner curvature vs. angle of attack; hulls enclose data linked to extant claw behavioural function from Thompson & Motani[69]; Roman numeral dots to terminal phalanges of digits I-V in *Eugyrinus*. Standardize colour codes in all three charts.



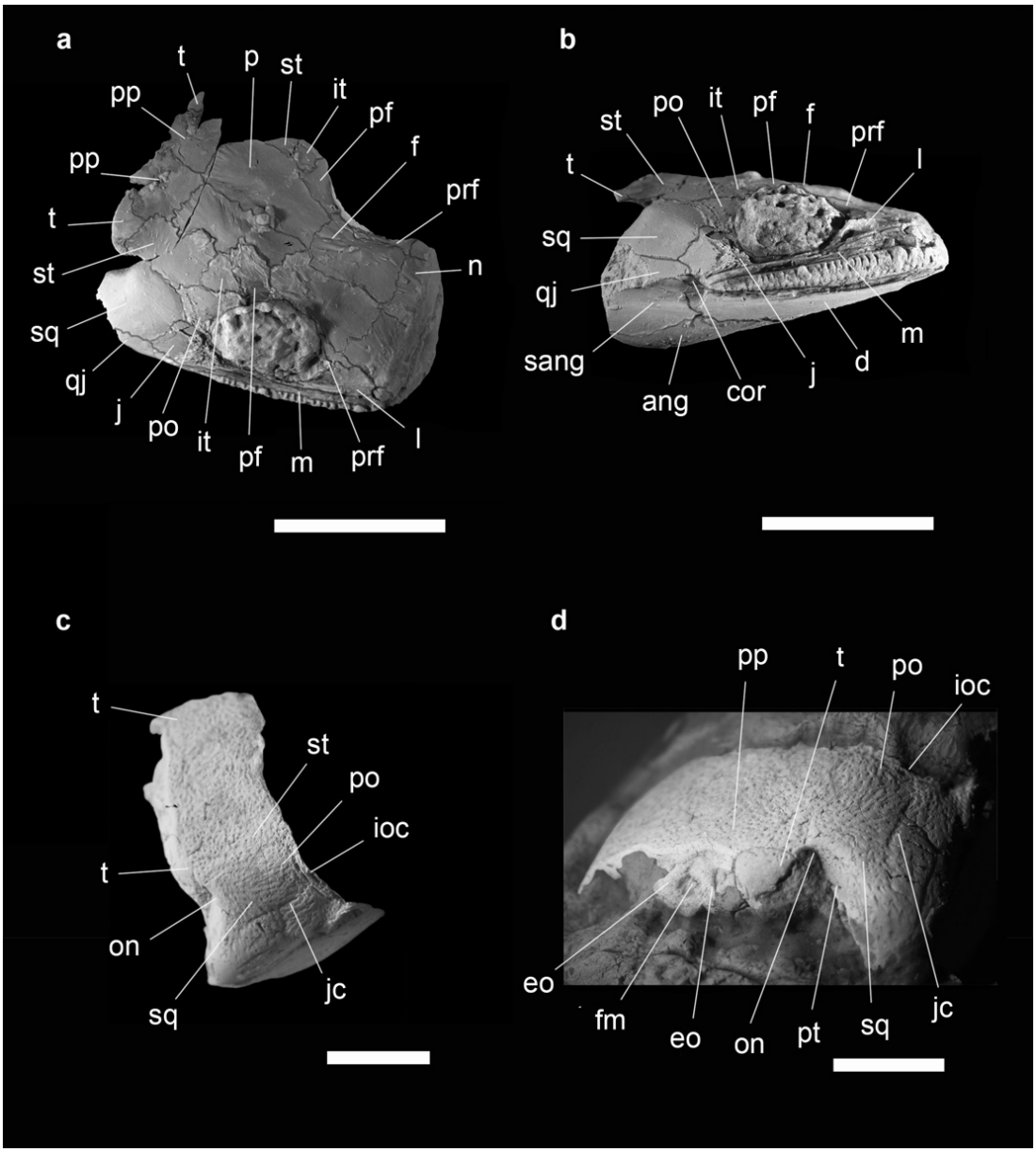
Extended Data Figure 1. *Eugyrinus wildi* (MANCH:W.1222). a, Entire specimen (photograph), part and **b**, counterpart. **c**, Skeletal reconstruction with minimal restoration (skull composite from natural moulds of external and mesial surfaces; hindlimb skeleton mirrored) in dorsal view; scales omitted. Scale bars 10 mm.



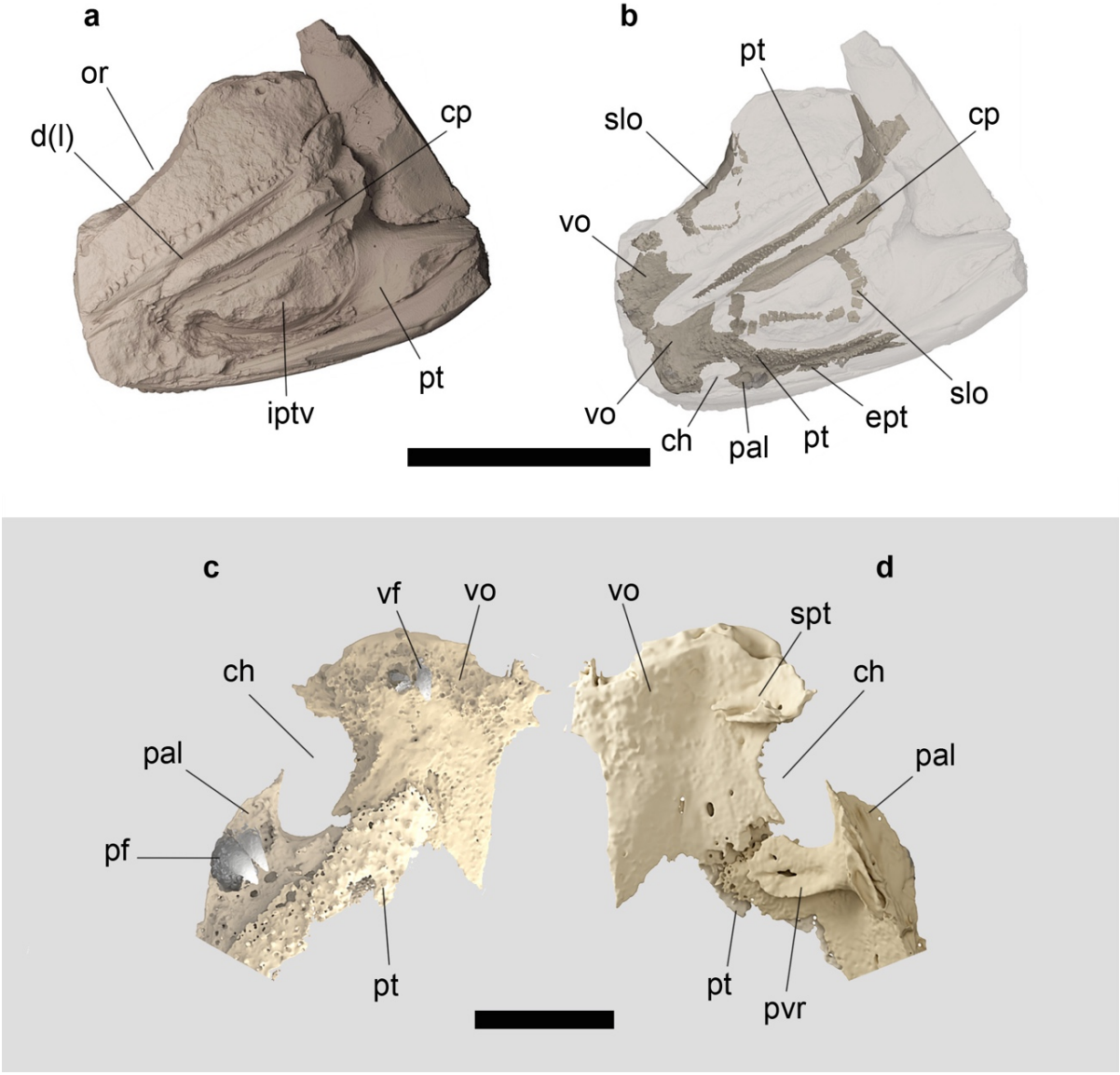
Extended Data Figure 2. *Eugyrinus wildi* (MANCH:W.1222), right forelimb and hindlimb. All paired images show structures in dorsal (left) and ventral (right) views; distal at top of figure. **a**, Ulna. **b**, Radius. **c**, Humerus. **d**, Forelimb reconstructed. **e**, Tibia. **f**, Fibula. **g**, Femur. **h**, Hindlimb reconstructed. **i,** distal view of hindlimb digits showing curvature of terminal phalanges. adc, adductor crest; ectf, ectepicondylar foramen; fbc, fibula crest; ol?, possible base of olecranon process. Scale bars 5mm (**a**-**c**, **e**-**g**), 5mm (**d**,**h,i**).



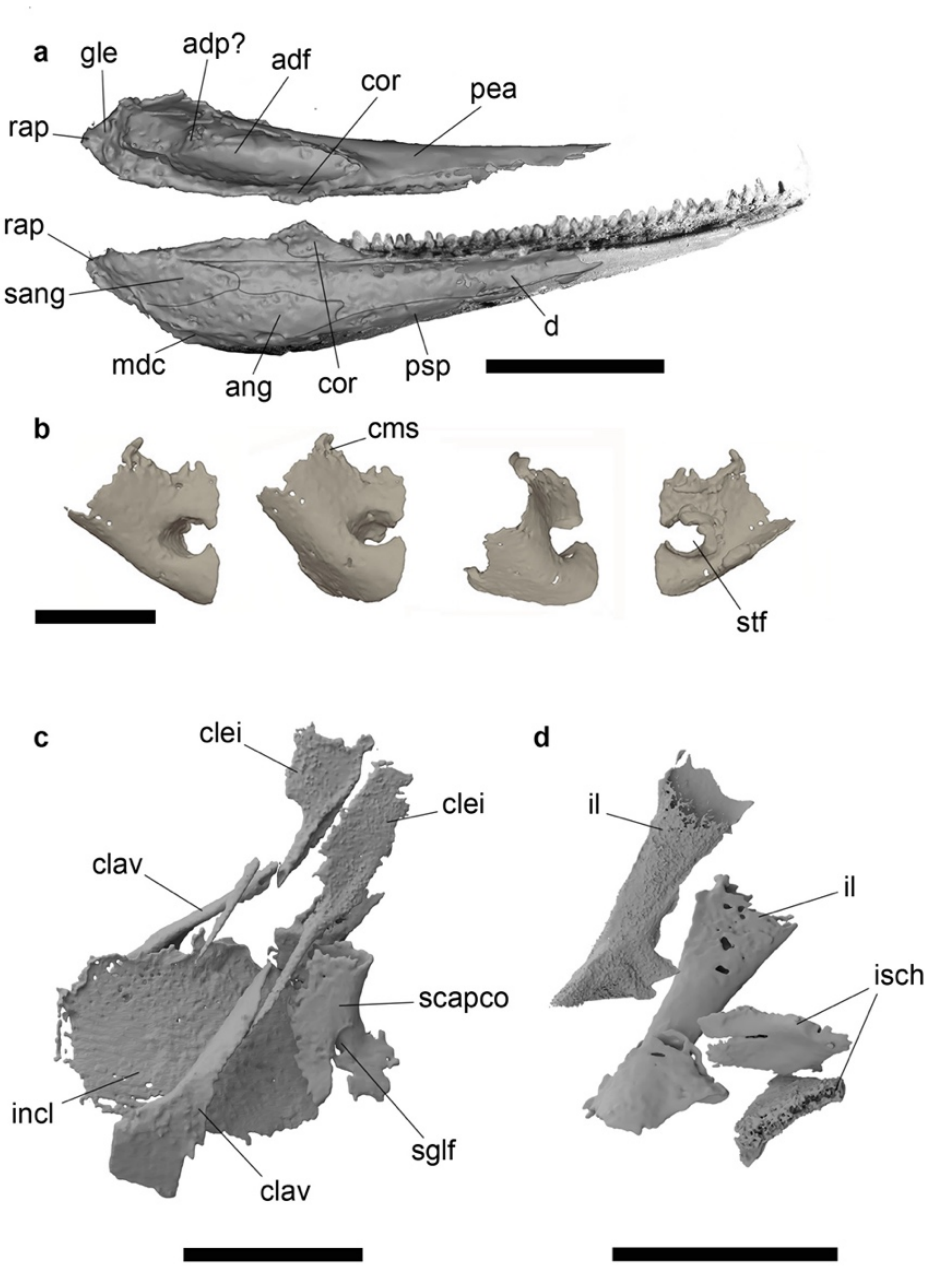
Extended Data Figure 3. *Eugyrinus wildi* (MANCH:W.1222), soft tissue preservation. a, CT cranial slice, horizontal, radiodense signal indicating path of olfactory tract and organ. **b**, Rendering of CT data showing olfactory tract and organ in lateral aspect. **c**, CT cranial slice, coronal, showing radiodense signal in right orbit. **d,** Rendering of CT data showing olfactory tract and organ in dorsal aspect. **e**-**h**, renderings of CT data showing volume of eyeball, retinal pigment epithelium, and collapsed ring of scleral ossicles in four aspects: anterior, ventromedial, dorsomedial, and laterodorsal. aqh, aqueous humour; ch, choana; nc, nasal cup; ns, nasal sac; ons, space for optic nerve; ot, olfactory tract; pal, palatine; pf, palatine fang; pt, pterygoid; pvr, palatine vomer ridge; rpe, retinal pigment epithelium; slo, scleral ossicles; spt, septomaxilla; tv, tubular vestibulum; vf, vomerine fang; vh, vitreous humour; vo, vomer. Scale bars 5 mm (**a**); 2 mm (**b**, **d**); 2.5 mm (**c**); 2.5 mm (**e**-**h**).



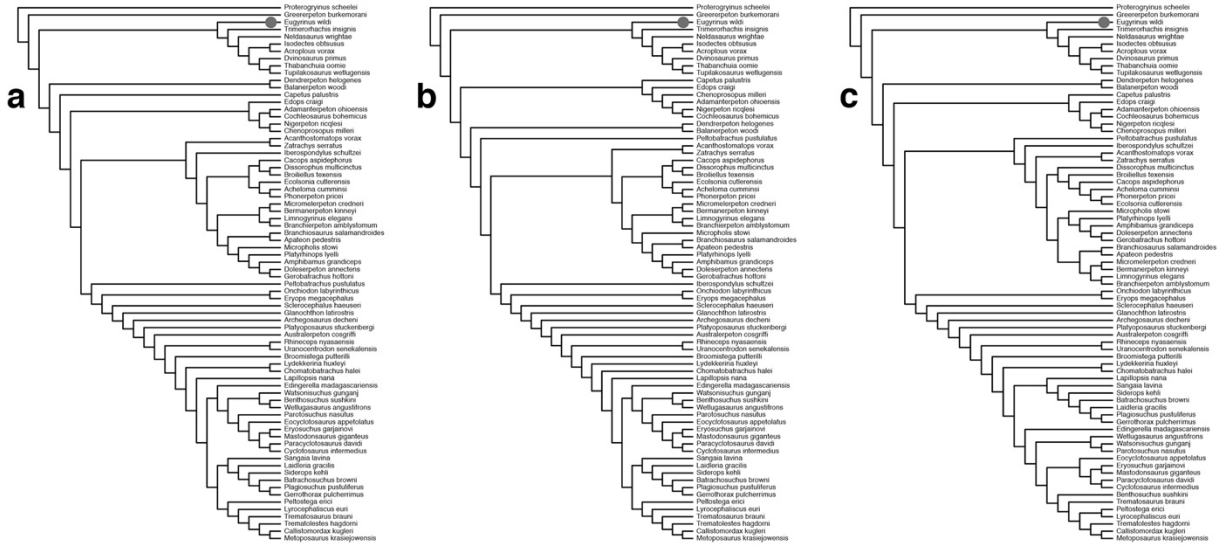
Extended Data Figure 4. ***Eugyrinus wildi*** **(MANCH:W.1222), cranium, external view. a,** Skull roof dorsolateral view, bones labeled. **b,** Skull, lateral view. **c,** Skull table and cheek, natural mould (peel). **d,** Otic notch and occipital detail from natural mould (peel). In parts **a** and **b** sutural boundaries are enhanced for clarity. Note that the visible surface, with minor exceptions, is the natural mould of the mesial surface of the dermatocranium. Although the skull is barely compressed dorsoventrally, it has undergone slight right-to-left side displacement, hence dislocated boundary between right temporal and parietal bones and slippage of left orbit beneath left frontal. ang, angular; cor, coronoid; d, dentary; eo, exoccipital; f, frontal; ioc, infraorbital canal; it, intertemporal; j, jugal; jc, jugular canal; l, lachrymal; m, maxilla; n, nasal; on, otic notch; p, parietal; po, postorbital; pp, postparietal; prf, prefrontal; pt, pterygoid; qj, quadratojugal; sang, surangular; sq, squamosal; st, supratemporal; t, tabular. Scale bars 10 mm (**a, b**); 5 mm (**c**, **d**).



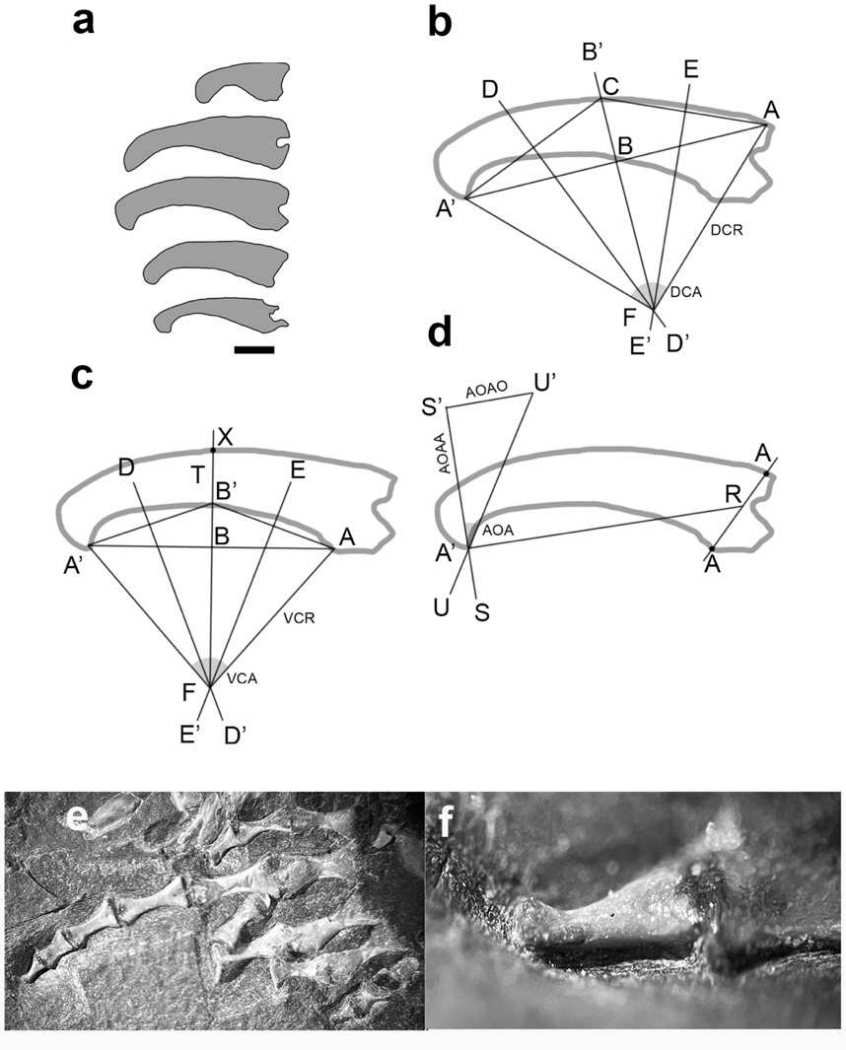
Extended Data Figure 5. ***Eugyrinus wildi*** **(MANCH:W.1222), cranium, CT renderings. a,** External surface of cranial block, ventral view showing natural mould of palate and left lower jaw. **b**, CT rendering showing detail of palate, choana, parasphenoid, scleral ossicles, in ventral (oral) view. **c**, Choana and surrounding vomer, palatine, ectopterygoid (part), and palatal ramus of pterygoid, in ventral (oral) view. **d**, Choana and surrounding bones including septmaxilla in dorsal view. ch, choana; cp, cultriform process of parasphenoid; d(l), dentary of left mandible; ept, ectopterygoid; iptv, interpterygoid vacuity; or, orbit; pal, palatine; palf, palatine fangs; pt, pterygoid; pvr, palatine vomer ridge; vf, vomerine fangs; vo, vomer; slo, scleral ossicles; spt, septomaxilla. Scale bars 10 mm (**a, b**); 2 mm (**c**, **d**).



Extended Data Figure 6. *Eugyrinus wildi* (MANCH:W.1222), mandible, stapes, and girdles. a, Lower jaw in dorsal and lateral aspects (lateral view: mosaic of CT rendering and specimen photograph). **b**, Stapes (right side) in four views, rotating from anterior to posterior. **c,** Pectoral girdle. **d**, Pelvic girdle. adf, adductor fossa; adp, adductor process; ang, angular; clav, clavicle; clei, cleithrum; cms, collumaris muscle scar; cor, coronoid process; d, dentary; gle, glenoid; il, iliac process; incl, interclavicle; isch, ischium; mdc, mandibular canal; pea, prearticular; psp, postsplenial; rap, retroarticular process; sang, surangular; scapco, scapulocoracoid; sgif, supraglenoid foramen; stf, stapedial foramen; Scale bars 5 mm (**a, c, d**); 1 mm (**b**).



Extended Data Figure 7. Results of phylogenetic analyses. a, Single most parsimonious tree recovered with reweighted and unordered characters. **b**, Single most parsimonious tree recovered with implied weights (concavity constant *K*=12) and unordered characters. **c**, Maximum clade credibility tree (50% majority-rule consensus) from uncalibrated Bayesian analysis. Blue dot marks the position of *Eugyrinus*.



Extended Data Fig. 8. *Eugyrinus wildi*, hindlimb terminal phalanx measurements (adapted from Mann et al. 2021 and Thomson and Motani 2021) and *Casineria kiddi,* forelimb terminal phalanx. a, Lateral outlines of *Eugyrinus* terminal phalanges I-V, ordered from top to bottom. Scale bar, 0.5mm. **b,** Measurement of dorsal curvature. **c,** Measurement of ventral curvature. **d,** Measurement of angle of attack. AOA, angle of attack; AOAA, angle of attack adjacent; AOAO, angle of attack opposite; DCA, dorsal claw angle; DCR, dorsal claw radius; VCA, ventral claw angle; VCR, ventral claw radius. **e**. *Casineria kiddi* (NMS G1993.54.1)[21], left manus. **f**, *Casineria kiddi* (NMS G1993.54.1), terminal phalanx of digit IV, left manus.

Extended Date Table 1. *Eugyrinus wildi*. Measurements (length in mm) of the articulated phalanges of the left pes.

Digit	Phalanx 1	Phalanx 2	Phalanx 3	Phalanx 4	Phalanx 5	Total
I	2	1.2	1.2			4.4
II	3.5	2.7	2.1			8.3

III	3.7	2.9	2.5	2.2		11.3
IV	3.3	3	2.6	2.1	1.8	12.8
V	2.3	2.3	2.1	1.6		8.3

Extended Data Table 2. *Eugyrinus wildi*. Measurements of curvature and thickness for each terminal phalanx of the pes. The final column provides averages for each row. The result in square brackets is the average for digits II-V (digit I terminal phalanx excluded). Measurements for claw radius and thickness in arbitrary units.

Digit	I	II	III	IV	V	Ave
DCA: Dorsal (Outer) Claw Angle	112	72	92	85	78	87.8 [81.8]
VCA: Ventral (Inner) Claw Angle	104	70	82	69	85	82 [76.5]
AOA: Angle of Attack	52	63	32	48	12	41.4 [38.8]
DCR: Dorsal Claw Radius	44	109	83	76	58	
VCR: Ventral Claw Radius	33	100	72	74	51	
T: Claw thickness	18	22	21	19	12	

Extended Data Table 3. Scan parameters use for computed X-ray microtomography.

Scan	Focus	Voxel size (um)	Voltage (kV)	Current (uA)	Timing (ms)	Projections	Filter
Whole 04643	Entire specimen at low resolution, used only for verification and alignment.	43.7360	130	200	333	1300	none
Anterior 04806	Focused on forelimbs, shoulder, and anterior axial column. Both part and counterpart.	24.8880	110	220	500	1900	none
Posterior 11721	Focused on pelvic girdle and posterior axial column. Both part and counterpart.	22.5700	120	190	500	2500	1.5 mm Cu
Hindlimbs 11770	Focused on hindlimbs, only part.	11.9260	120	100	1000	2100	.5 Sn
Head 13871	Isolated head - soft tissue, skull, palate	8.773	90	90	1000	2100	1.0mm Cu

Online Content

Any methods, additional references, Nature Research reporting summaries, source data, extended data, supplementary information, acknowledgements, peer review information; details of author contributions and competing interests; and statements of data and code availability are available at

Materials and Methods

Provenance. The single specimen of *Eugyrinus wildi* (Manchester Museum, Wild Collection, MANCH: W.1222) was collected by Mr George Wild circa 1888 from the Soapstone bed at Carry (Carre) Heys at Trawden[86]. Other, nodule-enclosed, three-dimensionally preserved vertebrates from the same locality and bed include the actinopterygians *Trawdenia planti*[38,39], *Mesonichthys aitkeni*[33,37], and *Coccocephalus wildi* [37,87]. Microsaurian remains are also noted[33]. The Soapstone bed occurs some 1.2m to 2.1m above the Mountain Four Feet coal[88] (also named Mountain 1.2m Coal; Lower Mountain Coal), but below the Arley Coal[39,89]. This correlates with the Westphalian A chronozone within the Langsettian substage of the Bashkirian stage[90]. The Mountain Four Feet coal seam is continuous with the 'Bullion' and 'Gannister' seams of the Burnley coal field[33], hence alternative descriptions of the *Eugyrinus* source as: from the roof of the Bullion Coal at Trawden[28]; from the marine roof of the Mountain Four-feet Mine of the Lower Coal-measures at Trawden[29]; from the Soapstone bed, Mountain Four-feet Mine, Carre Heys, Trawden[80]; from the Westphalian A of Colne[31]. Access to the Soapstone bed was likely via the long disused shaft near Carre Heys[33], unambiguously named Carry Heys on contemporary Ordnance Survey maps, located at National Grid Reference 390247.439729[39].

Computed X-ray microtomography, segmentation and three-dimensional rendering. The specimen, MANCH:W.1222, part, counterpart, and cranium, was scanned at the University of Chicago X-ray µCT facility, on a GE Phoenix 240/180 scanner using the 240 mode. Raw scan data were reconstructed with Phoenix datos|x and processed in VGStudioMax. Segmentation was accomplished using Materialise Mimics v.25. Virtual models were rendered using Blender 3.2 or Autodesk 3D StudioMax (Autodesk, Inc.) and were annotated in Adobe Photoshop 2024. Photography of fossils was accomplished with a Leica DFC490 camera attached to a Zeiss Stemi SV6 microscope. The initial scan of the complete specimen, used as a reference to align higher-resolution scans, was performed with parameters of 43.7360 µm using 130 kv, 200 mA, 333 ms timing, 1300 projections, and no filter. The anterior portion of both part and counterpart were scanned at a voxel size of 24.888 µm using 110 kv, 220 mA, 500 ms timing, 1900 projections, and no filter to visualize the bones of the anterior axial column, shoulder girdle, and forelimbs. The posterior portion of both part and counterpart were scanned at a voxel size of 22.5700 µm using 120 kv, 190 mA, 500 ms timing, 2500 projections, and a 1.5 mm Cu filter to visualize the pelvic girdle and posterior axial column. The hind limb region of the part specimen was scanned at a voxel size of 11.9260 µm using 120 kv, 100 mA, 1000 ms timing, 2100 projections, and a 0.5 mm Sn filter to achieve higher resolution of the foot. The isolated head was scanned at a voxel size of 8.773 µm using 90

kv, 90 mA, 1000 ms timing, 2100 projections, and a 1.0 mm Cu filter to visualize the soft tissues and bones of the skull and palate.

Phylogenetic analysis. Gee's[53] taxon-character set, an updated version of Schoch's[55] data matrix, formed the starting point for our phylogenetic analyses. All 207 discrete characters remained unchanged, but two temnospondyls were added: *Eugyrinus wildi* and *Bermanerpeton kinneyi* from the Late Pennsylvanian of New Mexico. Originally described by Werneburg et al.[47] as a dvinosaur, *Bermanerpeton* exhibts characteristics shared with dissorophoid groups such as branchiosaurids and larval amphibamids. Our resultant taxon list totals 72 temsnospondyl species representing a wide cross-section of the group's diversity, plus *Proterogyrinus* and *Greererpeton* as outgroups. We did not impose any order to characters except for those indicated in the original matrix, namely: 38, 65, 72-73, 99, 103-106, 132-133, 138, 140, 153, 158, 165, 177, 182, 186. This ordering scheme was followed in three of the parsimony analyses and in the uncalibrated Bayesian analysis.

Six parsimony analyses were carried out in PAUP* v. 4.0a.169[91]. Search settings differed only in the use of character ordering and weighting schemes; these matched those used by Gee[53] (Supplementary Information), and proceeded with the following treatments: characters unordered and unweighted/reweighted (unord_unw; unord_rew); characters ordered and unweighted/reweighted (ord_unw; ord_rew); characters unordered/ordered with implied weighting (K12_unord; K12_ord). Accordingly, we initially ran analyses with unweighted characters (i.e., equal unit weights), both unordered and ordered. Subsequently, characters were reweighted by the best fit value of their rescaled consistency index derived from the equally weighted searches. In addition, with both unordered and ordered characters, we utilised implied weights during tree searches[92,93]. In each case we used an arbitrary value of 12 for the constant of concavity *K*, a parameter controlling how strongly homoplastic characters ought to be downweighted in the course of tree optimization. Parsimony search settings were as follows: tree-bisection-reconnection branch swapping; $5{\cdot}10^5$ random stepwise taxon addition sequences; a single tree kept in memory at each stepwise addition; five subsequent rounds of branch swapping on all trees retained in memory at the end of the initial search; collapsing branches with minimum length of zero. When multiple equally parsimonious trees were obtained (both with ord_unw and unord_unw characters), results were summarized as strict consensus trees. Lastly, node support was evaluated through bootstrapping[94] and jackknifing[95] methods in PAUP*, in each case using 10^5 character-resampling replicates and 50% character deletion for jackknifing.

An uncalibrated Bayesian analysis was conducted using MrBayes v. 3.2.6[96], with the character ordering schemes in Gee[53]. The analysis was run for $2{\cdot}10^7$ generations (two independent runs; four chains). The

results, in the form of a 50% majority-rule consensus showing all groupings compatible with such consensus, were visualized with Figtree v. 1.4.4 (http://tree.bio.ed.ac.uk/software/figtree/). Analytical parameters followed examples from recent literature (e.g., Ford & Benson[84]). *Proterogyrinus* and *Greererpeton* were designated as successive outgroups to temnospondyls. For model specification, a gamma distribution was applied to accommodate rate heterogeneity among characters, allowing character-state transitions to vary across the dataset. Character coding was set to variable, excluding both constant and uninformative characters from the matrix[96].

PCA analysis. Drawn reconstructions of tetrapod hindlimbs were sourced from this study and the published literature; the full list of references is presented in the Supplementary Information. Sampling was broadly distributed across early amniotes, temnospondyls, and lepospondyls, focusing on taxa with good hindlimb data. Individual limb segments- autopod, stylopod, zeugopod- were measured in pixels using Affinity Designer 2. For each limb segment, the length of the segment was divided by the total length of the limb to produce a dataset of proportions. This dataset of proportions was subjected to a Principal Components Analysis (PCA) in RStudio for R[97,98]. The PCA was run using the stats package from base R[99]. The calculation was done via single value decomposition of the data matrix. Variables were scaled, centered, and rotated. PC1 and PC2 capture 66.82% and 33.18% of total variation, respectively. Plots were produced using the ggplot2[100], ggfortify[101], and ggrepel[102], and cluster[103] packages.

Claw Curvature Measurements. Measurements were taken from all five terminal phalanges of the hind limb using methods adopted after Mann et al.[7], Thomson and Motani[69], and references therein (see Extended Data Fig. 8 for graphic explanation). To measure the dorsal claw radius (DCR) and dorsal claw angle (DCA) a line was drawn from the extensor tubercle or proximal dorsal extremity (A) to the claw apex (A'). From the midpoint of the line AA' (B), a perpendicular line was then drawn that extended past the dorsal edge of the claw (B'). The intersection of this perpendicular line (BB') with the dorsal edge of the claw was defined as point C. Points A, C, and A' were connected to form an isosceles triangle. The lines CA and CA' were then bisected by perpendicular lines DD' and EE'; these symmetrical lines intersected at point F. Points A and A' were then connected to point F. The length of line FA provides the measure of DCR; the angle subtended by lines FA and FA' is the DCA. To measure ventral claw radius (VCR) and ventral claw angle (VCA) these methods were repeated but point A was placed at the flexor tubercle or proximal ventral extremity. Point B' was placed at the intersection of the line BB' with the ventral edge of the claw. To measure claw thickness (T) the line BB' was extended to the dorsal edge of the claw, the intersection defined as point X. T was defined by line length B'X.

To calculate the angle of attack the dorsoventral level of the mid-point of the articular joint, point R, was estimated by bisecting a line connecting points A in dorsal and ventral claw angle measurements (proximal dorsal and ventral extremities). A line was then drawn to point A', the claw apex, and a perpendicular line drawn from point A' (SS'). A line extending along the distalmost ventral edge of the claw (UU') approximated the angle of attack. A line perpendicular to SS' joined lines SS' and UU' (S'U'). The length of AS' was defined as AOAA (angle of attack adjacent), the length of S'U' as AOAO (angle of attack opposite), and the angle subtended by SS' and UU' as the AOA (angle of attack). The articular facets are not well preserved in *Eugyrinus*, and point R, the level of rotation, is a conservative estimate for each terminal phalanx. Moving point R proximally into the notional rotation centre of an articular joint results in more acute angle of attack; displacing point A' distally and ventrally to account for actual claw tip (see sections through *Xenopus* and *Mus* claws in Maddin et al.[27]), will increase AOA.

Data availability. The fossil described in this study is deposited in the collections of the Manchester Museum. All original scan datasets will be made publicly available and access information to the repository provided upon publication. For review purposes, we accept anonymized data sharing requests through the editorial office.

Acknowledgments We thank University of Manchester Museum, Drs D. Gelsthorpe, A. Edwards, Lindsey Loughtman, and K. Sherburn, for access to collections, specimen loan, and scan permission. We thank the National Museum of Scotland and Drs S. Walsh and N. Fraser for access to collections. We thank Clitheroe Castle Museum and C. Sutton for permission and assistance with collection searches. Invaluable fieldwork assistance was provided by Drs S. Giles, T. Smithson, and M. Webster. V. Venkataraman and L. Schnetz are thanked for discussion and insight. M.I.C. acknowledges support of NSF Research Grant IntBIO2433267. M.I.C. and A.C. receive funding and support from the University of Chicago. M.R. acknowledges funding from The Leverhulme Trust, RPG-2024-315.

Author contributions. M.I.C. lead the project and wrote the manuscript with contributions from B.K.A.O., A.M.C, and M.R. K.T. and A.M.C. undertook serial CT scans, analyses, and renderings with minor supplementary work by M.I.C. M.R. assembled the phylogenetic data set, completed analyses and provided associated supplementary materials. B.K.A.O. assembled data set of limb proportions and completed PCA analysis. M.I.C., A.M.C., K.T. and M.R. composed figures; A.M.C. assembled virtual reconstruction of *Eugyrinus* with input from M.I.C. All authors contributed to and edited the final draft.

Competing interests. The authors declare no competing interests.

References

1. Ruta, M. & Coates M. I. Dates, nodes and character conflict: addressing the lissamphibian origin problem. *J. Syst. Palaeontol.* **5**, 69-122 (2007).
2. Pardo, J. D., Szostakiwskyj, M., Ahlberg, P. E. & Anderson, J. S. Hidden morphological diversity among early tetrapods. *Nature* **546**, 642–645 (2017).
3. Clack, J. A. *Gaining Ground: The Origin and Evolution of Tetrapods* (Second Edition, Indiana University Press, Bloomington, 2012).
4. Schoch, R. *Amphibian Evolution: The Life of Early Land Vertebrates* (Wiley Blackwell, Chichester, 2014).
5. Carroll, R. L. *The Rise of Amphibians, 365 Million Years of Evolution* (The Johns Hopkins University Press, Baltimore, 2009).
6. Schoch, R. & Witzmann, F. The evolution of larvae in temnospondyls and the stepwise origin of amphibian metamorphosis. *Biol. Rev*. **99**, 1613–1637 (2024).
7. Mann, A., Dudgeon, T. W., Henrici, A. C., Berman, D. S. & Pierce, S. E. Digit and ungual morphology suggest adaptations for scansoriality in the Late Carboniferous eureptile *Anthracodromeus longipes*. *Front. Earth Sci.* **9**, 675337 (2021).
8. Spindler, F., Werneburg, R., Schneider, J. W., Luthardt, L., Annacker, V. & Rössler, R. *PalZ* **92**, 315–364 (2018).
9. Plikus, M. Intricately patterned scales of ancient skin. *Nature* **627**, 274–276 (2024).
10. Mooney, E. D., Maho, T., Bevitt, J. J. & Reisz, R. R. Paleozoic cave system preserves oldest-known evidence of amniote skin. *Current Biology* **34**, 417–426 (2024).
11. Maddin, H. C., Musat-Marcu, S. & Reisz, R. R. Histological microstructure of the claws of the African clawed frog, *Xenopus laevis* (Anura: Pipidae): implications for the evolution of claws in tetrapods. *J. Exp. Zool. B Mol. Dev. Evol.* **308**, 259–268 (2007).
12. Carron, M., Sachslehner, A. P., Cicekdal, M. B., Bruggeman, I., Demuynck, S., Golabi, B., De Baere, E., Declercq, W., Tschachler, E., Vleminckx, K. & Eckhart, L. Evolutionary origin of Hoxc15-dependent skin appendages in amphibians. *Nat. Commun.* **15**, 2328 (2024).
13. Di, R. et al. A mechano-resistance mechanism in skin adapts to terrestrial locomotion. *Cell* **188**, 1–12. (2025)

14. Milner A. R. & Sequeira S. E. K. The temnospondyl amphibians from the Visean of East Kirkton, West Lothian, Scotland. *Trans. R. Soc. Edinb. Earth Sci*. **84**, 331–361 (1993).
15. Long, J. A., Niedzwiedski, G., Garvey, J., Clement, A. M., Camens, A. B., Eury, C. A., Eason, J. & Ahlberg, P. E. Earliest amniote tracks recalibrate the timeline of tetrapod evolution. *Nature* **641**, 1193–1200 (2025).
16. Marsicano, C., Pardo, J. D., Smith, R. M. H., Mancuso, A., Gaetano, L. C. & Mocke, H. Giant stem tetrapod was apex predator in Gondwanan late Palaeozoic ice age. *Nature* **631**, 577–582 (2024).
17. Starck, J. M., Stewart, J. R. & Blackburn, D. G. Phylogeny and evolutionary history of the amniote egg. *J. Morph.* **282**, 1080–1122 (2021).
18. Clack, J. A. et al. Phylogenetic and environmental context of a Tournaisian tetrapod fauna. *Nat. Ecol. Evol.* **1**, 0002 (2016).
19. Stein, K., Prondvai, E., Huang, T., Baele, J.-M., Sander, P. M. & Reisz. Structure and evolutionary implications of the earliest (Sinemurian, Early Jurassic) dinosaur eggs and eggshells. *Sci. Rep*. **9**, 4424 (2019).
20. Klembara, J., Ruta, M., Anderson, J., Mayer, T., Hain, M. & Valaska, D. A redescription of *Brouffia orientalis* Carroll & Baird, 1972 from the Upper Carboniferous of the Czech Republic and the status and affinities of protorothyridid amniotes. *Swiss J. Palaeontol.* **143**, 33 (2024).
21. Paton, R. L., Smithson, T. R. & Clack, J. A. An amniote-like skeleton from the Early Carboniferous of Scotland. *Nature* **398**, 808–813 (1999).
22. Kennedy, N. K. Redescription of the postcranial skeleton of *Limnoscelis paludis* Williston (Diadectomorpha: Limnoscelidae) from the Upper Pennsylvanian of El Cobre Canyon, northern New Mexico. *Bull. N. M. Mus. Nat. Hist. Sci*. **49**, 211–220 (2010).
23. Clack, J. A., Smithson, T. R. & Ruta, M. A Mississippian (early Carboniferous) tetrapod showing early diversification of the hindlimbs. *Commun. Biol.* **5**, 238 (2022).
24. MacDougall M. J. et al. A new recumbirostran 'microsaur' from the Lower Permian Bromacker locality, Thuringia, Germany, and its fossorial adaptations. *Sci. Rep*. **14**, 4200 (2024).
25. Haslam, I. S., Roubos, E. W., Mangoni, M. L., Yoshizato, K., Vaudry, H., Kloepper, J. E., Pattwell, D. M., Maderson, P. F. A. & Paus, R. From frog integument to human skin: dermatological perspectives from frog skin biology. *Biol. Rev*. **89**, 618–655 (2014).
26. Cömden, E. A., Yennis, M. & Cakur, B. The complex bridge between aquatic and terrestrial life: skin changes during development of amphibians. *J. Dev. Biol.* **11**, 6 (2023).

27. Maddin, H. C., Eckhart, L., Jaeger, K., Russell, A. P. & Ghannadan, M. The anatomy and development of the claws of *Xenopus laevis* (Lissamphibia: Anura) reveal alternate pathways of structural evolution in the integument of tetrapods. *J. Anat*. **214**, 607–619 (2009).
28. Woodward, A. S. On a microsaurian (*Hylonomus wildi* sp. nov.) from the Lancashire coalfield. *Geol. Mag*. **8**, 211–213 (1891).
29. Watson, D. M. S. On *Eugyrinus wildi* (A. S. W.), a branchiosaur from the Lancashire Coal-Measures. *Geol. Mag*. **58**, 70–74 (1921).
30. Watson, D. M. S. The origin of frogs. *Trans. Roy. Soc. Edinb.* **60**, 195–231 (1940).
31. Milner, A. R. The temnospondyl amphibian *Dendrerpeton* from the Upper Carboniferous of Ireland. *Palaeontology* **23**, 125–141 (1980).
32. Schoch, R. R. & Milner, A. R. Temnospondyli; in Sues, H. D., ed., *Encyclopedia of Paleoherpetology* v.**3A**. Munich, Pfeil. 150 pp. (2015).
33. Bolton, H. Notes on the Geological Horizon and Palaeontology of the 'Soapstone Bed' in the Lower Coal-Measures near Colne, Lancashire. *Geol. Mag.* **V.II,** 433–437 (1905).
34. Sigurdsen, T. & Bolt, J. R. The Lower Permian amphibamid *Doleserpeton* (Temnospondyli: Dissorophoidea), the interrelationships of amphibamids, and the origin of modern amphibians. *J. Vertebr. Paleontol.* **30**, 1360–1377 (2010).
35. Pardo, J. D., Small, B. J. & Huttenlocker, A. K. Stem caecilian from the Triassic of Colorado sheds light on the origins of Lissamphibia. *Proc. Natl. Acad. Sci. USA*, **114**, e5389–e5395 (2017).
36. Marjanovic, D. & Laurin, M. Phylogeny of Paleozoic limbed vertebrates reassessed through revision and expansion of the largest published relevant data matrix. *PeerJ* **6**, e5565 (2019).
37. Figueroa, R. T., Goodvin, D., Kolmann, M. A., Coates, M. I., Caron, A. M., Friedman, M. & Giles, S. Exceptional fossil preservation and evolution of the ray-finned fish brain. *Nature* **614**, 486–491 (2023).
38. Coates, M. I. Endocranial preservation of a Carboniferous actinopterygian from Lancashire, UK, and the interrelationships of primitive actinopterygians. *Philos. Trans. R. Soc. B* **354**, 435–462 (1999).
39. Coates, M. I. & Tietjen, K. 'This strange little palaeoniscid': a new early actinopterygian genus, and a commentary on pectoral fin conditions and function. *Earth Environ. Sci. Trans. R. Soc. Edinb*. **109**, 15–31 (2018).
40. Caron. A., Tietjen, K. & Coates, M. I. Neural tissues and chondrostean traits in an early actinopterygian. *Nature*. Co-submission ms.

41. Panchen, A. L. The nostrils of choanae fishes and early tetrapods. *Biol. Revs* **42**, 374–420 (1967).
42. Dilkes, D. W. Biology and evolution of the nasal region in trematopoid amphibians. *Palaeontology* **36**, 839–854. (1993).
43. Ruta, M., Bolt, J. R. & Barber, L. J. Novel features and morphological variation in the lower jaw of the Permian temnospondyl amphibian *Trimerorhachis*. *Earth Environ. Sci. Trans. R. Soc. Edinb*. **115**, 185–211 (2025).
44. Arbez, T., Atkin, J. B. & Maddin, H. C. Cranial anatomy and systematics of *Dendrerpeton* cf. *helogenes* (Tetrapoda, Temnospondyli) from the Pennsylvanian of Joggins, revisited through micro-CT scanning. *Spec. Pap. Palaeontol*. **2022**, e1421 (2022).
45. Milner, A. R. A small temnospondyl amphibian from the Lower Pennsylvanian of Nova Scotia. *J. Paleontol*. **56**, 1302–1305 (1982).
46. Robinson, J., Ahlberg, P. E. & Koentges, G. The braincase and middle ear region of *Dendrerpeton acadianum* (Tetrapods: Temnospondyli). *Zool. J. Linn. Soc*. **143**, 577–597 (2005).
47. Werneburg, R., Schneider, J.W. & Lucas, S.G. The new dvinosaurian *Bermanerpeton kinneyi* (Temnospondyli), with “branchiosaurid” characters, from the late Pennsylvanian Kinney Brick Quarry in New Mexico. *Bull. N.M. Mus. Nat. Hist. Sci.* **84**, 433–452 (2021).
48. Holmes, R. B., Carroll, R. L. & Reisz, R. B. 1988. The first articulated skeleton of *Dendrerpeton acadianum* (Temnospondyli, Dendrerpetontidae) from the Lower Pennsylvanian Locality of Joggins, Nova Scotia, and a review of its relationships. *J. Vertebr. Paleontol.* **18**, 64–79 (1988).
49. Witzmann, F. The evolution of the scalation pattern in temnospondyl amphibians. *Zool. J. Linn. Soc*. **150**, 815–834 (2007).
50. Witzmann, F. Morphological and histological changes of dermal scales during the fish-to-tetrapod transition. *Acta Zool*. **92**, 281–302 (2011).
51. Dünker, N., Wake, M. H., & Olson, W. M. Embryonic and larval development in the caecilian *Ichthyophis kohtaoensis* (Amphibia, Gymnophiona): a staging table. *J. Morph.* **243**, 3–34 (2000).
52. Rogers, C. S., Astrop, T. I., Webb, S. M., Ito, S., Wakamatsu, K. & McNamara, M. E. Synchrotron X-ray absorption spectroscopy of melanosomes in vertebrates and cephalopods: implications for the affinity of *Tullimonstrum*. *Proc. R. Soc. B* **286**, 20191649 (2019).
53. Gee, B. M. *The disadvantage of derivation: conserved systematic flaws in primary data have repeatedly biased the phylogenetic inference of Temnospondyli (Tetrapoda, Amphibia).* bioRxiv. https://doi.org/10.1101/2022.06.22.496729. (2022).

54. Gee, B. M. & Sidor, C. A. Diminutive temnospondyls from the lower and middle Fremouw Formation (Lower Triassic) of Antarctica. *J. Vertebr. Paleontol.* **44**:2, e2407183, (2024).
55. Schoch, R. R. The evolution of major temnospondyl clades: an inclusive phylogenetic analysis. *J. Syst. Palaeontol.* **11**, 673–705. (2013).
56. Holmes, R. The Carboniferous amphibian *Proterogyrinus scheelei* Romer, and the early evolution of tetrapods. *Phil. Trans. R. Soc. Lond. B* **306**, 431–527 (1984).
57. Smithson, T. R. (1982). The cranial morphology of *Greererpeton burkemorani* Romer (Amphibia: Temnospondyli). *Zool. J. Linn. Soc.,* **76,** 29–90 (1982).
58. Godfrey, S. J. The postcranial skeleton of the Carboniferous tetrapod *Greererpeton burkemorani* Romer 1969. *Phil. Trans. R. Soc. Lond. B* **323**, 75–153 (1989).
59. Ruta, M. & Bolt, J. R. A reassessment of the temnospondyl amphibian *Perryella olsoni* from the Lower Permian of Oklahoma. *Trans. R. Soc. Edinb.: Earth Sci.* **97**, 113–165. (2006).
60. Milner A. R. A revision of the temnospondyl amphibians from the Upper Carboniferous of Joggins, Nova Scotia. *Spec. Pap. Palaeontol.* **52**, 81–103. (1996).
61. Sequeira, S. E. K. A cochleosaurid amphibian from the Upper Carboniferous of Ireland. *Spec. Pap. Palaeontol.* **52**, 65–80 (1996).
62. Garza, H. K., Catlos, E. J., Lapan, T. J., Clarke, J. A. & Brookfield, M. E. New U-Pb constrains and geochemisty of the East Kirkton Quarry, Scotland: implications for early tetrapod evolution in the Carboniferous. *PLoS ONE* **20** (4), e0321714 (2025).
63. Ruta, M., Witzmann, F., Klembara, J. & Fröbisch, N. Tempo and mode of skull size evolution in Temnospondyli (Tetrapoda: Amphibia) and lineage diversification in the largest group of early tetrapods. *Earth Environ. Sci. Trans. R. Soc. Edinb*. **115**, 212–234 (2025).
64. MacIver, M. A. & Finlay, B. L. The neuroecology of the water-to-land transition and the evolution of the vertebrate brain. *Phil. Trans. R. Soc. B* **377**, 20200523 (2021).
65. Clack, J. A., Smithson, T. R. & Ruta, M. A Mississippian (early Carboniferous) tetrapod showing early diversification of the hindlimbs. *Commun. Biol*. **5**, 283 (2022).
66. Wake, T. A., Wake, D. B. & Wake, M. H. The ossification sequence of *Aneides lugubris*, with comments on heterochrony. *J. Herpetol.* **17**, 10–22 (1983).
67. Brown, C. E., Sather, E. A., Dudley, R. & Deban, S. M. Gliding and parachuting by arboreal salamanders. *Curr. Biol.* **32**, R441–R456 (2022).

68. Birn-Jeffery, A. V., Miller, C. E., Naish, D., Rayfield, E. J. & Hone, D. W. E. Pedal claw curvature in birds, lizards, and Mesozoic dinosaurs – complicated categories and compensating for mass-specific and phylogenetic control. *PLoS One* **7**, e50555 (2012).

69. Thomson, T. J. & Motani, R. Functional morphology of vertebrate claws investigated using functionally based categories and multiple morphological metrics. *J. Morphol*. **282**, 449–471 (2021).

70. O'Connor, J., Clark, A., Kuo, P.-C., Kiat, Y., Fabbri, M., Shinya, A., Van Beek, C., Lu, J., Wang, M. & Hu, H. Chicago *Archaeopteryx* informs on the early evolution of the avian bauplan. *Nature* **641**, 1201–1207 (2025).

71. Stewart, T. A., Liang, C., Cotney, J. L., Noonan, J. P., Sanger, T. J. & Wagner, G. P. Evidence against tetrapod-wide digit identities and for a limited frame shift in bird wings. *Nat. Commun.* **10**, 3244 (2019).

72. Voigt, S., Berman, D. S. & Henrici, A. C. First well-established track-trackmaker association of Paleozoic tetrapods based on *Ichniotherium* trackways and diadectic skeletons from the Lower Permian of Germany. *J. Vertebr. Paleontol*. **27**, 553–570 (2007).

73. Dhouailly, D. et al. Getting to the root of scales, feather and hair: as deep as odontodes? *Exp. Dermatol*. **28**, 503–508 (2019).

74. Spiekman, S. N. F. et al. Triassic diapsid shows early diversification of skin appendages in reptiles. *Nature* **643**, 1297–1303 (2025).

75. Colbert, E. H. 1955. Scales of the Permian amphibian *Trimerorhachis*. *Am. Mus. Novit.* **1740**, 1–17.

76. Baeckens, S., Wainwright, D. K., Weaver, J. C., Irschick, D. J. & Losos, J. B. Ontogenetic scaling patterns of lizard skin surface structure as revealed by gel-based stereo-prolifometry. *J. Anat*. **235**, 346–356 (2019).

77. Fernald, R. D. in *Sensory Biology of Aquatic Animals* (eds. Atema, J. et al.) 435–467, (Springer, 1988).

78. Winkler, M., Shoa, G., Tran, S. T., Xie, Y., Thomasy, S., Raghunathan, V. K., Murphy, C., Brown, D. J. & Jester, J. V. A comparative study of vertebrate corneal structure: the evolution of a refractive lens. Invest. *Ophthalmol. Vis. Sci*. **56**, 2764–2772 (2015).

79. MacIver, M. A., Schmitz, L., Mugan, U., Murphey, T. D. & Mobley, C. D. Massive increase in visual range preceded the origin of terrestrial vertebrates. *Proc. Natl. Acad. Sci. USA*, **114**, e2375–e2384 (2017).

80. Wootton, R. Nymphs of Palaeodictyoptera (Insecta) from the Westphalian of England. *Palaeontology* **15**, 662–675 (1972).
81. Martinez et al. submitted. Olfaction reflects lifestyle transitions across tetrapods. *Science*. Co-submission ms.
82. Fillmore, D. L., Lucas, S. G. & Simpson, E. L. Ichnology of the Mississippian Mauch Chunk Formation, Eastern Pennsylvania. *Bull. New Mexico Mus. Nat. Hist. Sci*. **54**, 1–134 (2012).
83. Lucas, S. G., Stimson, M. R., King, O. A., Calder, J. H., Mansky, C. F., Hebert, B. L. & Hunt, A. P. in *The Carboniferous Timescale* (eds Lucas, S. G., Schneider, J. W., Wang, X. & Nikolaeva, S.) 933–963, (The Geological Society of London, 2021).
84. Ford, D. P. & Benson, R. B. J. The phylogeny of early amniotes and the affinities of Parareptilia and Varanopidae. *Nat. Ecol. Evol.* **4**, 57–65 (2020).
85. Marshall, J. E. A., Lakin, J., Troth, I. & Wallace-Johnson, S. M. UV-B radiation was the Devonian-Carboniferous boundary terrestrial extinction kill mechanism. *Sci. Adv.* **6**, eaba0768 (2020).
86. Wild, G. The Lower Coal Measures of Lancashire. *Trans. Manch. Geol. Soc.* **21**, 364–398 (1892).
87. Poplin, C. M. & Véran, M. A revision of the actinopterygian fish *Coccocephalus wildi* from the Upper Carboniferous of Lancashire. *Spec. Pap. Palaeontol.* **52**, 7–29 (1996).
88. Bolton, H. The Palaeontology of the Lancashire Coal Measures. Part 1. *Trans. Manch. Geol. and Min. Soc*. **28**, 378–415 (1904).
89. Hough, E. *Geology of the Burnley area (SD82NW and SD83SW)* (British Geological Survey, 2004).
90. Williamson, I. A. The Burnley Coalfield. *British Mining* **63**, 5–27 (1999).
91. Swofford, D. L. *Phylogenetic Analysis Using Parsimony (*and Other Methods)* (Sinaur Associates, Sunderland 1998).
92. Goloboff, P. A. Estimating character weights during tree search. *Cladistics* **9**, 83–89 (1993).
93. Goloboff, P. A., Torres Galvis, A. & Arias Becerra, J. S. Parsimony and model-based phylogenetic methods for morphological data: comments on O'Reilly et al. *Palaeontology* **61**, 625–630 (2018).
94. Felsenstein, J. Confidence limits on phylogenies: an approach using the bootstrap. *Evolution* **39**, 783–791 (1985).
95. Farris, J. S., Albert, V. A., Källersjö, M., Lipscomb, D. & Kluge, A. G. Parsimony jacknifing outperforms neighborjoining. *Cladistics* **12**, 99–124 (1996).
96. Ronquist, F. & Huelsenbeck, J. P. MrBayes 3: Bayesian phylogenetic inference under mixed models. *Bioinformatics* **12**, 1572–1574 (2003).

97. R Core Team. *R: A Language and Environment for Statistical Computing*. R Foundation for Statistical Computing (2024).
98. R Studio Team. *RStudio*. RStudio, Inc. (2024).
99. R Core Team. *The R Stats Package*. RStudio, Inc. (2024).
100. Wickham, H. *ggplot2: Elegant Graphics for Data Analysis*. Springer-Verlag (2016).
101. Tang, Y., Horikoshi, M. & Li, W. *ggfortify: Data Visualization Tools for Statistical Analysis Results*. (2016).
102. Slowikowski, K. *ggrepel: Automatically Position Non-Overlapping Text Labels with ggplot2* (2020).
103. Maechler, M., Rousseeuw, P., Struyf, A. & Hubert, M. '*Finding Groups in Data*': Cluster Analysis Extended Rousseeuw et al. 2.1.8.1 https://doi.org/10.32614/CRAN.package.cluster (1999).

Supplementary Information

Amniote traits and terrestriality in an early amphibian

Michael I. Coates[1], Benjamin K. A. Otoo[2], Abigail Caron[3], Kristen Tietjen[4], Marcello Ruta[5]

Supplementary Methods

Parsimony analyses

Six separate parsimony analyses were conducted in PAUP* v.4.0a169 (Swofford 1998). The analyses implied distinct regimes of character ordering and weighting, with ordered characters following Gee (2022). Accordingly, we examined the following treatments: (1) unordered characters with equal weights and with reweighting; (2) ordered characters with equal weights and with reweighting; and (3) unordered and ordered characters analysed under implied weighting. We first performed searches using equal character weights (unweighted analyses) under both unordered and ordered schemes. The resulting trees were then used to assign different weights to the characters (reweighted analyses), based upon their best-fit rescaled consistency index values. For both the ordered and unordered datasets, we additionally implemented implied weighting (Goloboff, 1993; Goloboff et al., 2008), using a concavity constant of $K = 12$. This follows common practice in applying moderate down-weighting to characters exhibiting substantial homoplasy during tree optimization (Goloboff et al., 2018).

All searches used the same heuristic settings: tree-bisection–reconnection (TBR) swapping, 5×10^5 random addition replicates with stepwise taxon addition, and retention of a single tree per replicate during the initial pass. The pool of trees collected at the end of this phase was then subjected to five further rounds of TBR swapping, and branches of zero length were collapsed. When multiple equally parsimonious topologies resulted, the outcomes were summarised using strict consensus trees.

Node support values for the equally weighted characters were estimated through bootstrap (Felsenstein, 1985) and jackknife character resampling (Farris et al., 1996). A fast stepwise addition sequence was applied in both cases, producing 10^5 pseudoreplicates in PAUP*, and deleting 50% of characters for jackknife sampling. Only clades with frequencies of 50% or greater were retained in the bootstrap and jackknife majority-rule consensus, with bootstrap and jackknife support (hereafter, b.s. and j.s.) appended to its branches.

Bayesian analysis

Introductory notes. Bayesian phylogenetic analyses use Markov Chain Monte Carlo (MCMC) sampling to explore tree space and approximate the posterior distribution of tree topologies and model parameters. The analyses proceed through tree space in a series of steps, sampling trees in proportion to their fit to the data. Each of these sampled sequences constitutes a 'chain'. Typically, multiple chains are run in parallel – one 'cold' chain and several 'heated' chains. Heated chains move more freely through tree space and occasionally exchange states with the cold chain, thereby improving tree space exploration and reducing the risk of the analysis becoming confined to a single region of that space. Running multiple chains also provides an internal check on reliability, whereby independently sampled chains should converge on the same posterior distribution (Ronquist & Huelsenbeck 2003).

To evaluate convergence, several diagnostics are provided. The Potential Scale Reduction Factor (PSRF) assesses whether independent chains sample the same underlying distribution (i.e., whether they sample the same region of parameter space) by comparing variation within chains to variation between them. Values close to 1.00 indicate good convergence. The Estimated Sample Size (ESS) measures the effective number of independent samples obtained during the MCMC run. Because successive samples are autocorrelated, the total number of sampled trees is not equivalent to the number of independent observations. ESS adjusts for this dependence, with values above ~200 typically indicating that the posterior distribution has been sampled adequately (i.e., chains contain enough independent information). When both metrics fall within acceptable ranges, the resulting posterior estimates can be interpreted with confidence (Gelman & Rubin 1992; Brooks & Gelman 1998).

Settings. An uncalibrated Bayesian analysis was carried out in MrBayes v.3 (Ronquist & Huelsenbeck 2003). Rate variation across characters was modelled using a gamma distribution, allowing different morphological characters to evolve at different rates (*rates = gamma*). Characters showing no variation across taxa – i.e., phylogenetically uninformative – were excluded (*coding = variable*). Two topological constraints were enforced. First, the colosteid *Greererpeton burkemorani* was constrained to form the immediate outgroup to temnospondyls, with the embolomere *Proterogyrinus scheelei* specified as a more distant outgroup (*outgroup Proterogryinus_scheelei*). Second, temnospondyls were constrained to be monophyletic (*constraint ingroup1 = 2-74*; *constraint ingroup2 = 3-74*; *prset topologypr = constraints (ingroup1,ingroup2)*). Ordering of characters followed Gee (2022); for brevity, no analysis using unordered characters was performed.

The analysis consisted of two independent runs (*nrun = 2*), each comprising four chains (*nchain = 4*). A relatively low heating parameter (*temp = 0.1*) was used to improve chain mixing by increasing the

likelihood of swaps among chains. The MCMC chains were run for 2×10^7 million generations (*ngen = 20000000*), with trees and parameter values sampled every 1,000 generations (*samplefreq = 1000*) and diagnostic information printed at the same interval (*printfreq = 1000*). Convergence diagnostics were calculated every 5,000 generations (*diagnfreq = 5000*). Tree branch lengths were stored for all sampled trees (*savebrlens = yes*). A relative burn-in of 25% (*relburnin = yes burninfrac = 0.25*) was discarded before summarising posterior samples, ensuring that only the stationary portion of each chain contributed to the final parameter estimates.

A summary of posterior tree distribution was obtained using the *sumt* command. A majority-rule consensus with compatible partitioning was produced (*contype = allcompat*), including all clades present in at least 50% of the post-burn-in samples, together with any additional compatible groupings. Trees were written in FigTree-compatible format (*conformat = Figtree*). A summary of posterior parameter estimates was obtained with the *sump* command, again discarding the initial 25% burn-in prior to calculating posterior summary statistics and convergence diagnostics.

Supplementary Results

The results of our phylogenetic analyses broadly concur on the branching pattern between and within major temnospondyl clades, but they also differ in the relative position of some groups and underscore the instability of a few taxa (for discussions of conflicting topologies, see Gee 2022 and Gee & Sidor 2024). Owing to this instability, these taxa are often recovered outside the groups to which they have traditionally been assigned. Among the groups and species that are most prone to inconsistent phylogenetic placement are Dendrerpetidae (*Balanerpeton* woodi + *Dendrerpeton helogenes*), *Capetus palustris*, *Iberospondylus schultzei*, *Lapillopsis nana*, and *Peltobatrachus pustulatus*.

Parsimony topologies

The six maximum-parsimony analyses (Extended Data Fig. 7a,b and Supplementary Figs. 1 and 2) illustrate the strong influence of character weighting – whether through *a posteriori* reweighting or implied weighting – on the degree of phylogenetic resolution. In addition, bootstrap and jackknife character resampling emphasize the generally low statistical support for many groups (Supplementary Figs. 3 and 4). Equal-weights (‘unweighted’) analyses return multiple shortest trees (Supplementary Figs. 1a and 2a), whereas each weighted analysis yields a single optimal tree (Extended Data Fig. 7a,b and Supplementary Figs. 1b and 2b). Ordering the 17 characters identified by Gee (2022) (Supplementary Table 1) has only a modest impact on tree topology compared with the effects of weighting. Moreover, when characters are left unordered, the unweighted analysis produces fewer equally most parsimonious

887 trees and a better-resolved strict consensus (Supplementary Fig. 2a) than when characters are ordered
888 (Supplementary Fig. 1a). Most of this additional resolution primarily pertains to the radiation of
889 Eryopiformes (Schoch 2013), the group comprising Eryopidae (*Eryops megacephalus* + *Onchiodon*
890 *labyrinthicus*) and Stereospondylomorpha (*Sclerocephalus haeuseri* and all more apical taxa).
891 In all single trees recovered from the weighted analysis, the branching sequence of major groups
892 – excluding unstable taxa – is as follows: (Dvinosauria + (Edopoidea + ((Zatracheidae + Dissorophoidea) +
893 Eryopiformes))). Across these analyses, Dendrerpetidae occupy one of two positions: either immediately
894 crownward of Dvinosauria or crownward of Edopoidea. Under the first of these patterns, *Capetus* lies
895 immediately crownward of Dendrerpetidae, and *Peltobatrachus* forms the sister taxon to Eryopiformes
896 (Extended Data Fig. 7a). Under the second pattern, *Capetus* is retrieved as the sister taxon to Edopoidea,
897 and *Peltobatrachus* occurs immediately crownward of Dendrerpetidae (Extended Data Fig. 7b and
898 Supplementary Figs. 1b and 2b). In the same analyses, *Iberospondylus* is placed either as the sister taxon
899 to Dissorophoidea (Extended Data Fig. 7a and Supplementary Fig. 1b) or as the sister taxon to
900 Eryopiformes (Extended Data Fig. 7b and Supplementary Fig. 2b). *Lapillopsis* is recovered in several
901 alternative positions: as the sister taxon to a heterogeneous grouping of 'higher' Stereospondyli
902 (Extended Data Fig. 7a,b), as sister to Eryopiformes (Supplementary Fig. 1b), or nested withing 'higher'
903 Stereospondyli at the base of a diverse clade including Plagiosauridae (*Gerrothorax pulcherrimus*;
904 *Plagiosuchus pustuliferus*), Brachyopidae (*Batrachosuchus browni*), Chigutisauridae (*Siderops kehli*), and
905 'Rhytidosteidae' (*Laidleria gracilis*; *Sangaia lavinai*) (Supplementary Fig. 2b).
906 The weighted analyses also reveal numerous conflicting branching patterns within major groups,
907 with the exception of Dvinosauria (see below). Conflict is particularly pronounced within
908 Dissorophoidea, where several different patterns of interrelationships among the constituent subclades
909 are recovered. Within Dissorophoidea, only the clade Olsoniformes shows consistent internal structure,
910 with Dissorophidae (*Cacops aspidephorus* + (*Dissorophus multicinctus* + *Broiliellus texensis*)) as the siter
911 group to Trematopidae (*Ecolsonia cutlerensis* + (*Acheloma cumminsi* + *Phonerpeton pricei*)). In most
912 analyses, Olsoniformes form the sister group to remaining Dissorophoidea, but in the analysis based
913 upon reweighted and ordered characters, they occupy an intermediate position between
914 Micromelerpetidae (*Micromelerpeton credneri* + (*Branchierpeton amblystomum* + *Limnogyrinus*
915 *elegans*)) and Amphibamiformes (Supplementary Fig. 1b). Both the monophyly of Micromelerpetidae
916 (see below for comments on *Bermanerpeton kinneyi*) and the branching order among component taxa
917 are found in all weighted analyses. However, in both unweighted analyses (Supplementary Figs. 1a and

2a), Micromelerpetidae are resolved as a paraphyletic grade with respect to Branchiosauridae (*Branchiosaurus salamandroides* + *Apateon pedestris*).

Only a small number of clades receive strong bootstrap and jackknife support. These include Zatracheidae (*Acanthostomatops vorax* + *Zatrachys serratus*; b.s. = 90%; j.s. = 89%), Eryopidae (b.s. = 99%; j.s. = 98%), Plagiosauridae (b.s. = 94%; j.s. = 93%), Olsoniformes (b.s. = 94%; j.s. = 93%), and Tupilakosauridae (*Thabanchuia oomie* + *Tupilakosaurus wetlugensis*; b.s. = 86%; j.s. = 85%). Several other clades receive are only moderately or weakly supported, including Edopoidea (b.s. = 72%; j.s. = 69%), Dissorophoidea (b.s. = 58%; j.s. = 56%), and Dvinosauroidea (i.e., all dvinosaurs more apical than *Trimerorhachis* and *Neldasaurus*) (b.s. = 52%; j.s. = 50%).

Bayesian topology

The maximum clade credibility tree from the uncalibrated Bayesian analysis reveals several branching arrangements that depart from those recovered under parsimony (Supplementary Fig. 5). Notable examples include the placement of *Peltobatrachus* and *Iberospondylus* as successive sister taxa – in that order – to the clade (Zatracheidae + Dissorophoidea), as well as the recovery of Dissorophidae as a paraphyletic array relative to Trematopidae. In other respects, the Bayesian tree aligns most closely with the parsimony topologies generated under reweighted and implied-weights analyses using ordered characters (Supplementary Figs. 1b and 2b). Posterior probability values along the 'backbone' of the tree are generally high, apart from a few internal branches within Capitosauria.

Supplementary Discussion

***Eugyrinus* and Dvinosauria**

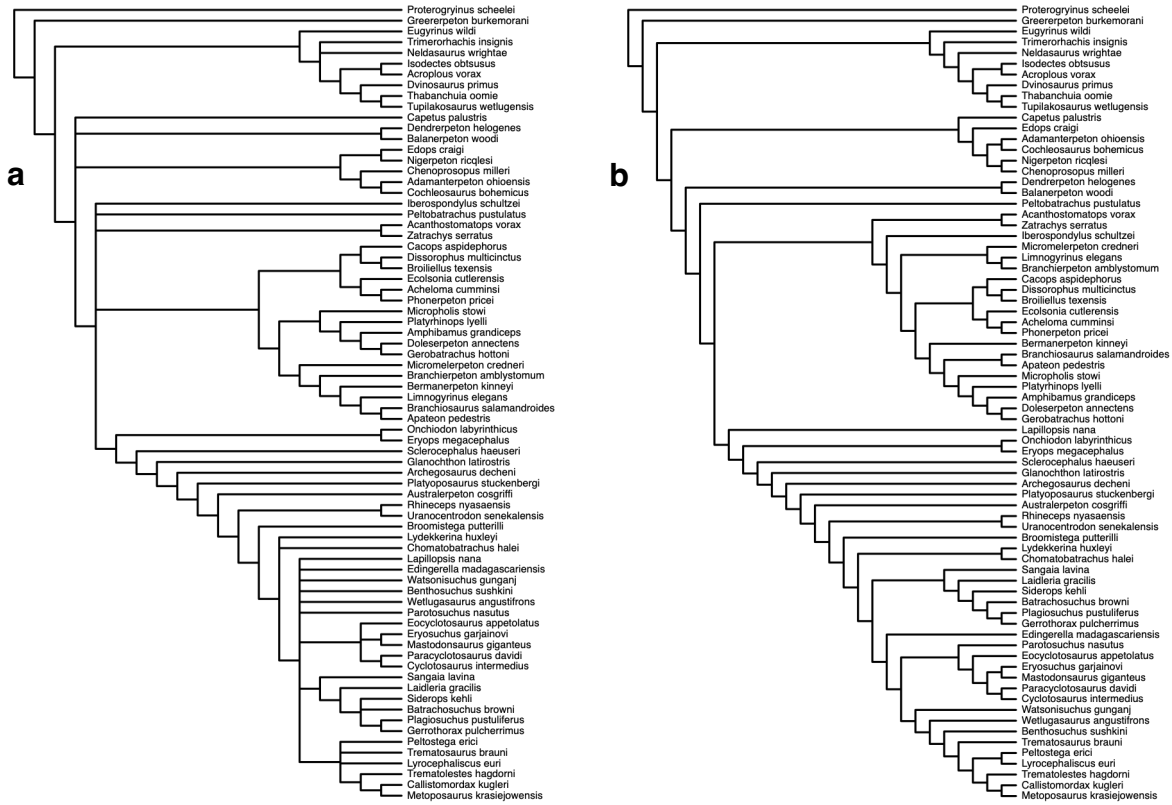
Across all parsimony and Bayesian analyses, *Eugyrinus wildi* is placed as sister taxon to remaining Dvinosauria. This clade forms the earliest diverging radiation of temnospondyls and, except in the analysis with unweighted and ordered characters (Supplementary Fig. 1a), its internal relationships are fully resolved. It does not receive support in the 50% majority-rule bootstrap and jackknife consensus topologies (Supplementary Figs. 3 and 4), but it is strongly supported in the Bayesian analysis (p.p. = 1) (Supplementary Fig. 5). The internal relationships of Dvinosauria conform to the arrangement retrieved in most phylogenetic analyses, with Trimerorhachidae (*Trimerorhachis insignis*; *Neldasaurus wrightae*) as the earliest diverging forms, and with remaining taxa – the Dvinosauroidea – consisting of Eobrachyopidae (*Acroplous* vorax; *Isodectes obtusus*), Dvinosauridae (*Dvinosaurus primus*), and Tupilakosauridae (*Thabanchuia oomie*; *Tupilakosaurus wetlugensis*) in increasingly more apical

949 succession. Within Dvinosauria, strong Bayesian support is assigned the branch uniting all taxa more
950 apical than *Eugyrinus* (p.p = 0.98) and to the branch subtending Dvinosauroidea (p.p = 0.99).
951 **A note on *Bermanerpeton***
952 As part of ongoing work on the interrelationships of temnospondyls, we decided to test the affinities of
953 *Bermanerpeton kinneyi*, a late Pennsylvanian taxon originally described as a dvinosaur exhibiting
954 characters in common with branchiosaurid dissorophoids (Werneburg et al. 2021). Our analyses fail to
955 support this assignment. Instead, *Bermanerpeton* emerges as a dissorophoid, although its precise
956 placement remains ambiguous. In most weighted parsimony analyses, as well as in the Bayesian analysis,
957 this taxon is nested within Micromelerpetidae as sister group to *Micromelerpeton* (Extended Data Fig. 7
958 and Supplementary Figs. 2b and 4). In the unweighted parsimony analyses, *Bermanerpeton* is part of a
959 paraphyletic array of Micromelerpetidae placed adjacent to Branchiosauridae (Supplementary Figs. 1a
960 and 2a). In the analysis with reweighted and ordered characters, however, *Bermanerpeton* is retrieved in
961 a more apical position, as the sister taxon to Amphibamiformes (Supplementary Figs. 1b). Lastly, the
962 sister-taxon relationship between *Bermanerpeton* and *Micromelerpeton* is also found in the Bayesian
963 analysis, although it receives low support (p.p. = 0.57) (Supplementary Fig. 5).
964

965 **Supplementary Figures**

966

967 Supplementary Figure 1. Results of parsimony phylogenetic analyses 1.



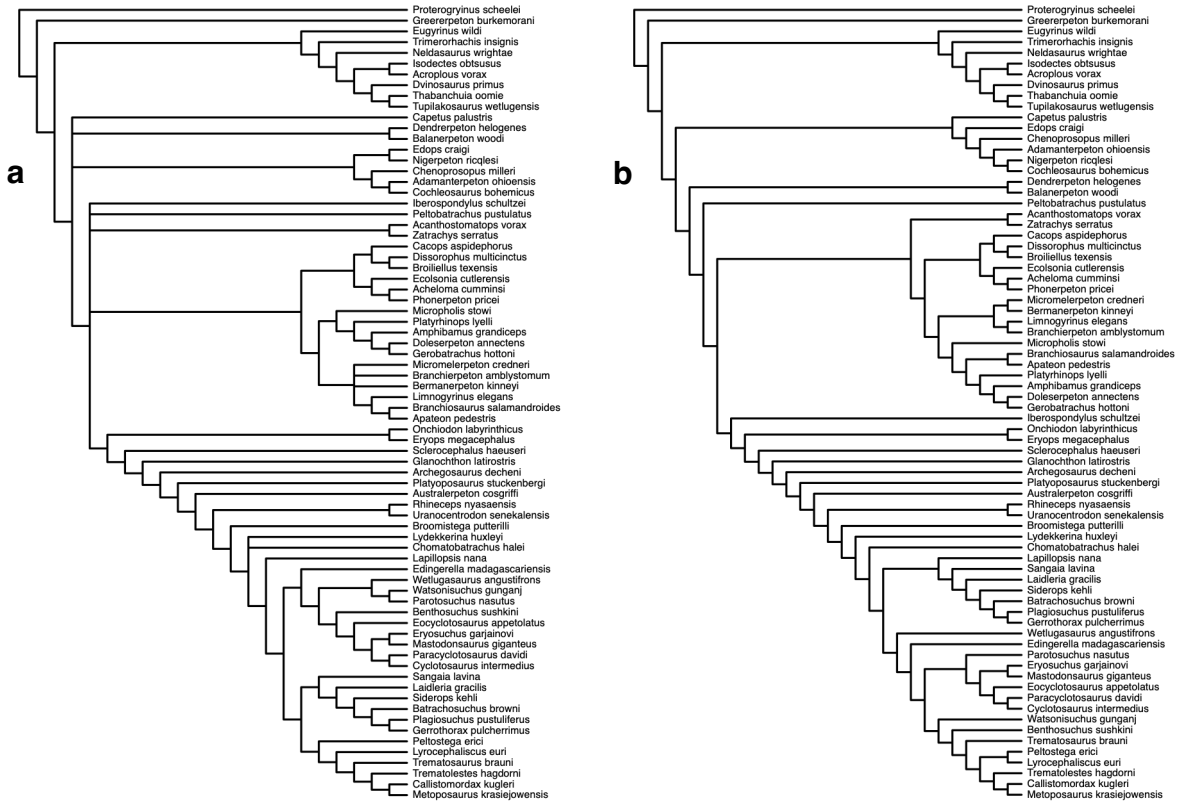
968

969 **a**, Strict consensus of 306 most parsimonious tree recovered with unweighted and ordered characters. **b**,

970 Single most parsimonious tree recovered with reweighted and ordered characters.

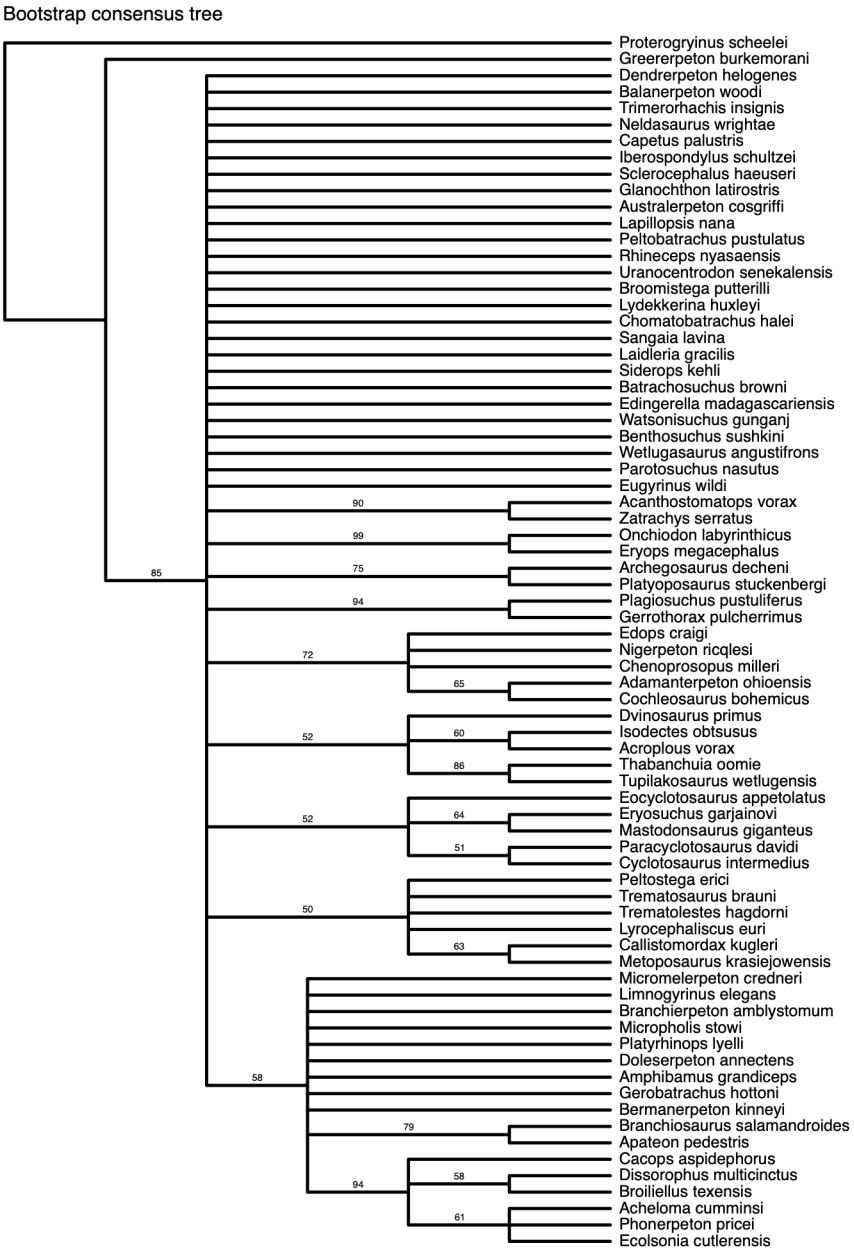
971

Supplementary Figure 2. Results of parsimony phylogenetic analyses 2.



a, Strict consensus of 84 most parsimonious tree recovered with unweighted and unordered characters. **b**, Single most parsimonious tree recovered with implied weights (concavity constant *K*=12) and ordered characters.

978 Supplementary Figure 3. Bootstrap 50% majority-rule consensus.

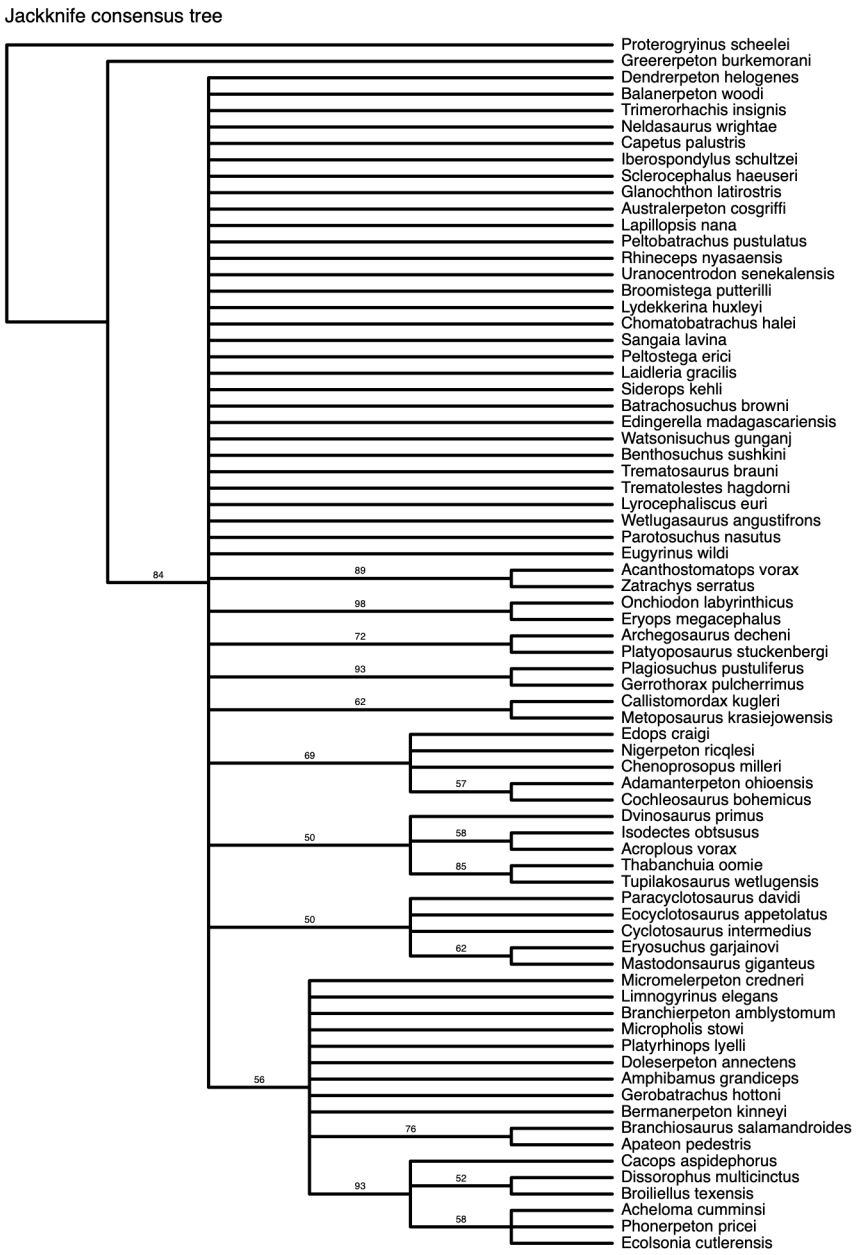


979

980 Numbers above branches represent bootstrap percentage support.

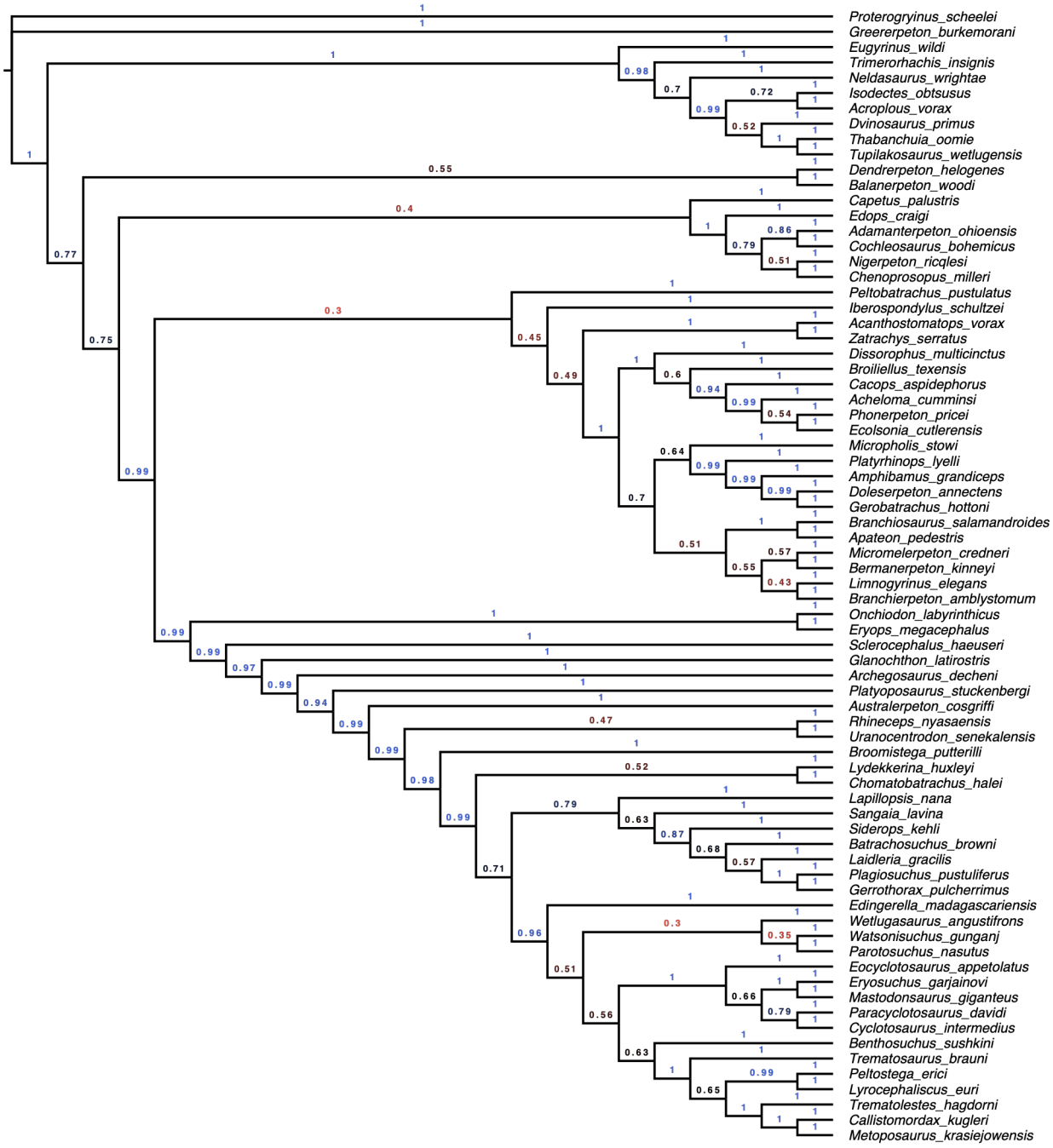
981

982 Supplementary Figure 4. Jackknife 50% majority-rule consensus.



983
984 Numbers above branches represent jackknife percentage support.
985

Supplementary Figure 5. Results of uncalibrated Bayesian phylogenetic analysis.



Maximum clade credibility tree (50% majority-rule consensus) from uncalibrated Bayesian analysis; colour-coded numbers above branches represent Bayesian posterior probabilities (red = lowest probability value; blue = highest probability value; tones along red-blue gradient = intermediate probability values).

Supplementary Tables

Supplementary Table 1. Basic tree statistics from parsimony analyses.

PARSIMONY ANALYSES	number of trees	tree length	C.I.	R.I.	R.C.	Goloboff fit
1. Equally weighted characters; ordered characters as specified below	306	1008	0.2512	0.7004	0.1786	–
2. All characters reweighted by maximum r.c. from **1**; ordered characters as specified below	1	173.75605	0.4665	0.8536	0.4113	–
3. Equally weighted characters; all characters unordered	84	998	0.2538	0.6993	0.1801	–
4. All characters reweighted by maximum r.c. from **3**; all characters unordered	1	171.1568	0.4758	0.8544	0.4195	–
5. Implied weighting with *K* = 12; ordered characters as specified below	1	1012	0.2502	0.6988	0.1775	-163.8591
6. Implied weighting with *K* = 12; all characters unordered	1	1002	0.2528	0.6976	0.1789	-164.2036
ordered characters: 38, 65, 72, 73, 99, 103, 106, 132, 133, 138, 140, 153, 158, 165, 177, 182, 186						
C.I. = ensemble Consistency Index, excluding uninformative characters						
R.I. = ensemble Retention Index						
R.C.= ensemble Rescaled Consistency Index						
r.c. = rescaled consistency index of individual characters						
K = Goloboff's constant of concavity						

For each of the six parsimony analyses, number of resulting shortest trees, tree lengths, and measures of character fit are reported.

Supplementary Table 2. Model parameter summary from Bayesian analysis.

BAYESIAN ANALYSIS																		
			95% HPD Interval															
Parameter	Mean	Variance	Lower	Upper	Median	min ESS	avg ESS	PSRF										
TL	7.026931	0.338471	5.932734	8.202636	7.003101	13500.94	13735.74	1										
alpha	0.748236	0.018983	0.486339	1.016415	0.737451	13826.8	14049.11	1										
TL= sum of all branch lengths, i.e., the total amount of evolutionary change across the tree for any given MCMC sample																		
alpha = parameter controlling the shape of the gamma distribution of rates of character change across tree branches																		
ESS = Effective Sample Size, measuring sampling efficiency within each chain, i.e., whether enough effective samples have been reached)																		
PSRF = Potential Scale Reduction Factor, measuring agreement between chains, i.e., how effectively they converge towards the same target distribution)																		
HPD = Highest Posterior Density Interval, i.e., the narrowest possible interval that captures 95% of the posterior probability of a parameter (range pf parameter values with the highest posterior support)																		

For both TL and alpha parameters, posterior summary statistics and convergence diagnostics are reported.

Supplementary References

Swofford, D. L. *Phylogenetic Analysis Using Parsimony (*and Other Methods)* (Sinaur Associates, Sunderland 1998).

Gee, B. M. *The disadvantage of derivation: conserved systematic flaws in primary data have repeatedly biased the phylogenetic inference of Temnospondyli (Tetrapoda, Amphibia).* bioRxiv. https://doi.org/10.1101/2022.06.22.496729. (2022).

Goloboff, P. A. Estimating character weights during tree search. *Cladistics* **9**, 83–89 (1993).

Goloboff, P. A., Carpenter, J. M., Arias, J. S. & Miranda-Esquivel, D. R. 2008. Weighting against homoplasy improves phylogenetic analysis of morphological datasets. *Cladistics* **24**, 1–16 (2008).

Goloboff, P. A., Torres, A., & Arias, J. S. Weighted parsimony outperforms other methods of phylogenetic inference under models appropriate for morphology. *Cladistics* **34**, 407–437 (2018).

1014 Felsenstein, J. Confidence limits on phylogenies: an approach using the bootstrap. *Evolution* **39**, 783–791
1015 (1985).
1016 Farris, J. S., Albert, V. A., Källersjö, M., Lipscomb, D. & Kluge, A. G. Parsimony jackknifing outperforms
1017 neighbour-joining. *Cladistics* **12**, 99–124 (1996).
1018 Ronquist, F. & Huelsenbeck, J. P. MrBayes 3: Bayesian phylogenetic inference under mixed models.
1019 *Bioinformatics* **19**, 1572–1574 (2003).
1020 Gelman, A. & Rubin, D. B. Inference from iterative simulation using multiple sequences.
1021 *Stat. Sci*. **7**, 457–472 (1992).
1022 Brooks, S. P. & Gelman, A. General methods for monitoring convergence of iterative simulations. *J.*
1023 *Comput. Graph. Stat*. **7**, 434–455 (1998).
1024 Gee, B. M. & Sidor, C. A. Diminutive temnospondyls from the lower and middle Fremouw Formation (Lower
1025 Triassic) of Antarctica. *J. Vertebr. Paleontol.* **44**:2, e2407183, (2024).
1026 Schoch, R. R. The evolution of major temnospondyl clades: an inclusive phylogenetic analysis. *J. Syst.*
1027 *Palaeontol.* **11**, 673–705 (2013).
1028 Werneburg, R., Schneider, J.W. & Lucas, S.G. The new dvinosaurian *Bermanerpeton kinneyi*
1029 (Temnospondyli), with “branchiosaurid” characters, from the late Pennsylvanian Kinney Brick
1030 Quarry in New Mexico. *Bull. N.M. Mus. Nat. Hist. Sci.* **84**, 433–452 (2021).
1031
1032 **Data matrix (nexus file) for phylogenetic analyses**
1033 **Spreadsheet of limb measurements for PCA plot**
1034